Probing phase transitions in neutron stars via the crust-core interfacial mode

Jiaxiang Zhu,[1] Chuming Wang,[1] Chengjun Xia,[2] Enping Zhou,[3,*] and Yiqiu Ma[1,3,†]

[1]Center for Gravitational Experiments, Hubei Key Laboratory of Gravitation and Quantum Physics, School of Physics, Huazhong University of Science and Technology, Wuhan, 430074, People's Republic of China

[2]Department of Physics, Yangzhou University, Yangzhou, Jiangsu, People's Republic of China

[3]Department of Astronomy, School of Physics, Huazhong University of Science and Technology, Wuhan, 430074, People's Republic of China

(Received 19 November 2022; accepted 27 March 2023; published 18 April 2023)

Gravitational waves emitted from the binary neutron star (BNS) systems can carry information about the dense matter phase in these compact stars. The crust-core interfacial mode is an oscillation mode in a neutron star, and it depends mostly on the equation of state of the matter in the crust-core transition region. This mode can be resonantly excited by the tidal field of an inspiraling-in BNS system, thereby affecting the emitted gravitational waves and hence could be used to probe the equation of state in the crust-core transition region. In this work, we investigate, in detail, how the first-order phase transition inside the neutron star, if it exists, affects the properties of the crust-core interfacial mode using a Newtonian fluid perturbation theory on a general relativistic background solution of the stellar structure. Two possible types of phase transitions are considered: (1) the phase transitions happen in the fluid core but near the crust-core interface, which results in density discontinuities, and (2) the strong interaction phase transitions in the dense core (as in the conventional hybrid star case). We study how these phase transitions affect the properties of the neutron star oscillation mode excited at the interface, where there exists a shear modulus discontinuity (interfacial mode). In particular, the former phase transition has a minor effect on the mass-radius relation, and the adiabatic tidal deformability, but has the potential to significantly affect the interfacial mode frequency and thereby could be probed using gravitational waves. For the BNS systems, we discuss the possible observational signatures of these phase transitions in the gravitational waveforms and their detectability. Our work enriches the exploration of the physical properties of the crust-core interfacial mode and provides a promising method for probing the phase transition using the seismology of a compact star.

DOI: 10.1103/PhysRevD.107.083023

I. INTRODUCTION

Quantum chromodynamics is nonperturbative at low energy scales, therefore, understanding the equation of state (EOS) and the phase transition of dense matter around 1–10 times the nuclear saturation density from the first principle is an issue. Currently, models based on microscopic many-body theories and energy density functional theories are used to describe the dense matter, while there are still many uncertainties about these theories due to the complexity of the nonperturbative strong interaction. Nuclear physics experiments in the Earth's laboratory have a limited capability to unveil cold dense nuclear matter above the nuclear saturation density [1–6]. Developing methods to probe these matter states and test the microscopic theories is important for understanding dense matter.

Compact stars, such as neutron stars (NSs) or hybrid stars (HSs), can carry information about these dense matters. A neutron star has a rich and interesting structure [7], typically consisting of a surface ocean (which is a plasma consisting of free electrons and ions), a solid crust with dramatic density profile ($d\rho(r)/dr \sim 10^9$ g/cm^4), and a neutron-fluid core. This solid crust can be divided into two regions: the several hundred-meters thick outer crust with density up to the neutron-drip density ($\rho_{\rm drip} \sim 10^{11}$ g/cm^3); the inner crust consists of neutron-rich nuclei, free neutrons and some electrons and protons, with density ranging from the neutron-drip density to the nuclear saturation density ($\rho_{\rm sat} \sim 2.5 \times 10^{14}$ g/cm^3 or number density equal to 0.15 fm^{-3}). In the crust-core transition region, the nuclear matter is so dense that exotic nuclear states could form, such as nuclear pasta, nuclear waffles [8–11], etc. These exotic nuclear matter states are generated by the competition between the Coulomb force and the nuclear force. Inside the core, for the region where the fluid density is lower than

*ezhou@hust.edu.cn
†myqphy@hust.edu.cn

$10\rho_{\rm sat}$ but higher than the nuclear pasta density, there could also be phase transitions due to the emergence of new baryon states. The onset densities for heavier baryons and quarks degrees of freedom are still unclear with model predictions ranging from $2\rho_{\rm sat}$ to $10\rho_{\rm sat}$, while those new degrees of freedom are competing with each other. Moreover, if there exists a quark core inside the compact star, then this type of compact star is named as a "hybrid star." It has been shown that the possible phase transition in the dense matter, although with uncertain microscopic modeling, could leave detectable imprints in the postmerger gravitational wave (GW) waveform of binary neutron star (BNS) systems, and the prospects of verifying such a scenario is also suggested [12–14].

These compact stars, containing dense matter with a density higher than the nuclear saturation density, are a natural laboratory for probing these dense matter states. Measurements of NS mass and radius play an important role in constraining the EOS of NSs [15–24]. Recently, the discovery of GWs radiated from BNS systems opened a new window for probing the EOS of the dense matter: firstly, information such as NS tidal deformability is encoded in the inspiral GW signals [25–28]; secondly, the electromagnetic counterparts of a BNS merger depend sensitively on the merger outcome, which constrains many EOS properties [29–33].

In this work, we focus on using NS/HS seismology to probe the first-order phase transitions inside NSs. A similar discussion has been proposed by Lau *et al.* [34], where they investigated the interfacial mode excited at the interface between the crystalline quark core and the neutron fluid in a HS. In their case, the typical frequency of the interfacial mode is ∼500 Hz, which is a relatively high band for current ground-based gravitational wave detectors. Compared to Lau *et al.* [34], our work has the following different features: (1) We focus on the interfacial mode excited at the interface between NS crust and the neutron fluid core [35–37], the frequency of which is typically a lower frequency band, therefore, being more observationally feasible. (2) Regarding the NS, we are interested in probing the signature of the first-order phase transition of dense matter near the crust-core interface by investigating how the crust-core interfacial mode will be affected by this phase transition. It is interesting that these first-order phase transitions could have a very minor effect on the mass-radius (M-R) relation and tidal deformability. Therefore, the gravitational wave signatures associated with the interfacial mode is a promising channel to probe these phase transitions. (3) Regarding the HS with quark core, we are interested in probing the high-density matter states by distinguishing the so-called "twin-star" phenomenon in the M-R relation, which is due to the introduction of the hadron-quark phase transition [38]. In this case, the two components of the twin star will have different radii and structures, though their masses are the same. Therefore, the interfacial mode and the corresponding GW phenomenology will also be different, which provides an observational possibility to study the phase transition of the strong-interaction matter. In addition, there are also other works [39] investigating the effect of phase transitions inside the crust on the oscillation mode in a hot adolescent/newborn NS in a general relativistic framework, and the effect of the cooling process of a hot NS on the crust shear modes is also studied.

The structure of this paper is the following: Section II introduces the phase transitions in the compact star and its effect on the M-R relations; Section III discusses the properties of interfacial modes and how they are affected by the phase transition; Section IV is devoted to investigating the coupling of the interfacial modes to the orbital motion of binary compact star systems and how to use the associated gravitational wave observation to probe these phase transitions; Finally, we will conclude the paper and present an outlook. The appendices will present the details of solving interfacial mode and the approach to the crust melting process.

II. PHASE TRANSITIONS OF THE HIGH DENSITY NUCLEAR MATTER

A. Hadron-quark phase transition and the twin-star scenario

Phase transition in the core of a compact star can change its M-R relation. This phenomenon has been investigated in [38], where they discussed the generic conditions for stable hybrid stars, assuming that the surface tension of the phase

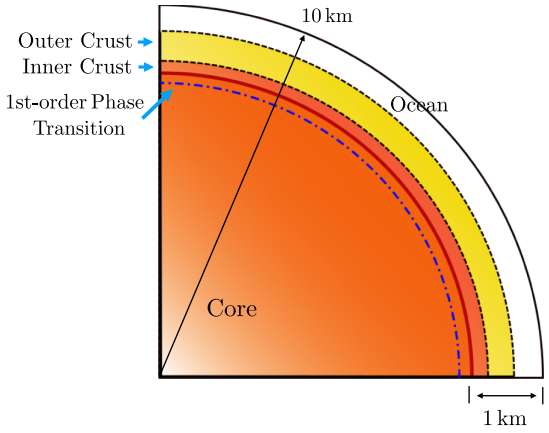

FIG. 1. Relevant neutron star structure for the interfacial modes are discussed in this paper. The outer crust consists of a dense Coulomb crystal, while the inner crust consists of dense nuclei. The nuclear pasta phase is located at the bottom of the inner crust, with only ∼100 meters thickness. The density of the inner crust ranges from the neutron drip density to the nuclear saturation density. Inside the neutron star fluid core, depending on the EOS, there could be a first-order phase transition (denoted as blue dot-dashed lines) in the fluid core near the crust-core interface, where new baryon states could emerge. In the deeper region of the core, a first-order phase transition from the hadronic matter state to the quark matter state can happen.

boundary is high enough to prevent the formation of a mixed phase. Such a boundary at the interface between hadronic matter and quark matter could exist in the NS core in Fig. 1. The general structure of the EOS we use is shown in Fig. 2, where the hadronic matter phase and quark matter phase are connected by a first-order phase transition.

In the high-density region, we adopt the constant speed of sound (CSS) model to describe the quark matter [38,40]. The CSS model has a feature in which the sound speed in the quark matter is almost constant, which is independent of the baryon number density. This feature is exhibited in many microscopic quark models (as summarized in [40]), e.g., the perturbative quark matter EOS [41] with a roughly constant $c^2_{\rm QM} \approx 0.2$–0.3, the model based on the field correlator method [42], and some variations of the MIT bag model or Nambu–Jona-Lasinio models [43,44]. Concretely, the CSS EOS is described by the following relation [38]:

$$\begin{aligned} \rho(p) &= \rho_{\rm trans} + \Delta\rho + c^{-2}_{\rm QM}(p - p_{\rm trans}), \\ p(\mu_B) &= A\mu_B^{1+1/c^2_{\rm QM}} - B, \\ \mu_B(p) &= [(p+B)/A]^{c^2_{\rm QM}/(1+c^2_{\rm QM})}, \\ n(\mu_B) &= (1+1/c^2_{\rm QM})A\mu_B^{1/c^2_{\rm QM}}, \end{aligned} \tag{1}$$

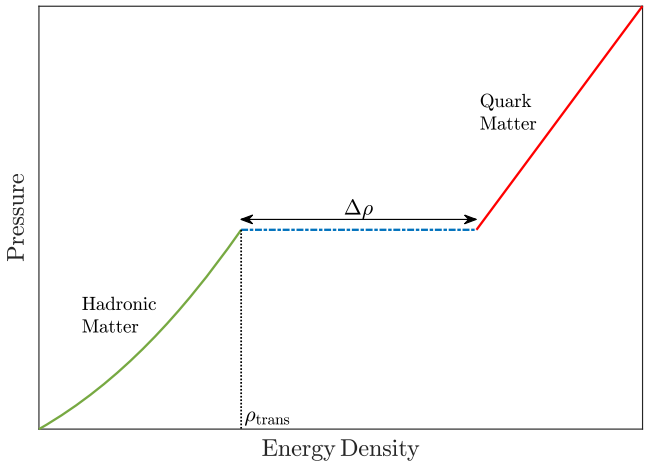

FIG. 2. Illustration of an equation of state model involving a hadron-quark first-order phase transition. The red line in the high energy density region represents the quark matter phase, while the green line in the low energy density region represents the hadronic matter phase. In between, there exists a first-order phase transition starting at $\rho_{\rm trans} = 5.2429 \times 10^{14}$ g/cm^3 with width $\Delta\rho = 5.8720 \times 10^{14}$ g/cm^3, using the NL3 EOS for the hadronic matter. Note that here and in Sec. III B, we use the NL3 EOS for illustrative purposes since the NL3 is a very stiff EOS and the two components of the corresponding twin-star solution (Fig. 3) have a relatively large radius difference. This means the effect of the quark core on the interfacial mode will be more significant (see Sec. III B). The EOS in Table I can also be stiff (e.g., DD-LZ1), but the radius difference of the twin-star components is relatively small. This EOS corresponds to the twin-star solution of $1.6M_\odot$ in Fig. 3.

where ρ, p, μ_B, n are the energy density, pressure, chemical potential, and the baryon number density, respectively. The $\rho_{\rm trans}, \Delta\rho, c_{\rm QM}$ are the energy density at the phase transition point, the energy density width of the phase transition, and the sound speed of the quark matter, respectively. The coefficient $B = (\rho_{\rm trans} + \Delta\rho - c^{-2}_{\rm QM}p_{\rm trans})/(1 + c^{-2}_{\rm QM})$ is determined by the quark deconfinement transition point (See Appendix A in Ref. [38] for a detailed proof), and A is an undetermined constant whose value does not affect the energy density-pressure relation. For hadronic matter phase on the lower density region, we adopt the models based on the nonrelativistic/relativistic mean-field theories [45]. By specifying that the μ_B remains constant during the hadron-quark first-order phase transition, we can determine the coefficient A mentioned above and thus determine the number density n; in this way we connect the nuclear matter and quark matter.

With different parameters, different M-R relations can be obtained using the above EOS and the Tolman-Oppenheimer-Volkoff (TOV) equations [38]. The interesting parameter space corresponds to the so-called disconnected hybrid stars, as shown in Fig. 3 as an example where we used the covariant density functional NL3 [46] for the hadronic matter and the CSS model for the quark matter. We choose

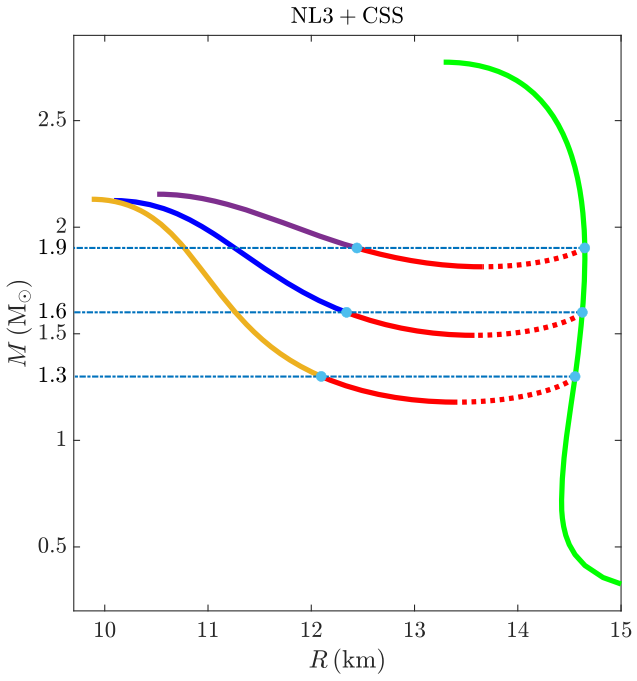

FIG. 3. M-R for the hybrid star with nuclear-quark transition in the core. This disconnected M-R relation exists for certain phase transition parameters with a large energy density jump $\Delta\rho/\rho_{\rm trans}$ and medium $\rho_{\rm trans}$. The twin-star solution for three different masses $M = (1.3M_\odot, 1.6M_\odot, 1.9M_\odot)$ and three different EOSs are shown. The dashed lines represent the unstable HS configuration. The EOSs of the quark core and the nuclear matter are the CSS model and NL3 model, respectively.

TABLE I. Upper panel: the interfacial mode frequency for a $1.4M_\odot$ neutron star computed using different EOS models partially based on the CompOSE database. The density discontinuity is set to happen at $n = 0.1$ fm^{-3}. The $n_{\rm trans}$ is the baryon number density at which the shear modulus transition happens, which is obtained from the corresponding microscopic models of the EOS.[a] The $\Delta\rho/\rho$ is the relative width of the first-order phase transition plateau. The $f_{i_{\mu/\rho}}$ and $f_{\tilde{i}_{\mu/\rho}}$ are the frequencies of the interfacial mode $i_{\mu/\rho}$ before and after we introduce their interactions, respectively. We can see that the interaction induces the avoiding crossing of the modes as discussed in the main text. Lower panel: pictorial demonstration of the avoiding crossing of the modes.

EOS	SKI6 [47]	RS [48]	SLY4 [49]	APR4 [50]	DD2 [51,52]	DDME2 [53–55]	TW [56]	DD-LZ1 [57]
$n_{\rm trans}$(fm^{-3})	0.0895	0.0672	0.076	0.0672	0.067	0.074	0.076	0.07
$\Delta\rho/\rho$	1.47%	3.41%	5.19%	7.36%	1.52%	3.30%	5.06%	7.24%
f_{i_μ} (Hz)	49.2	41.8	54.2	50.3	50.0	56.0	56.8	56.3
$f_{\tilde{i}_\mu}$ (Hz) (1st PT)	23.9	33.4	36.3	36	37.2	37.1	40.3	36.9
f_{i_ρ} (Hz)	81.6	154.3	152.6	183.7	91.2	128.7	166.5	172.5
$f_{\tilde{i}_\rho}$ (Hz) (with shear)	91.9	156.0	157.7	186.5	97.6	135.6	171.4	177.6

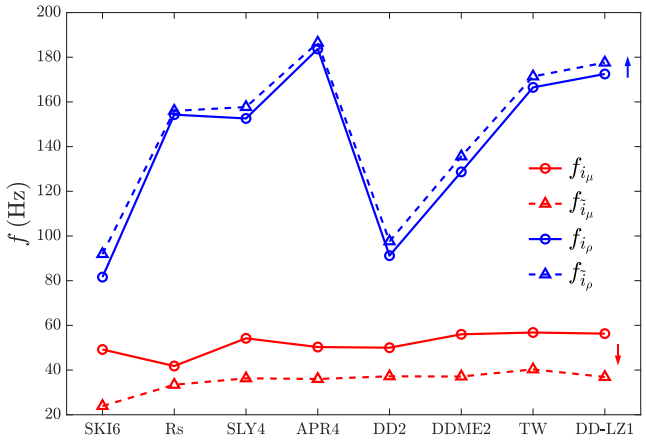

[a]For the EOS data, see the CompOSE website: https://compose.obspm.fr. In the composition table, we choose the $n_{\rm trans}$ to be the density where the proton number Z and the nuclei number A are zero, which is the upper limit density at which the nuclei structure disappears.

the NL3 EOS for the illustrative purpose since the two component stars in the twin-star solution have a relatively large difference compared to other EOSs in Table I. For a compact star with a fixed mass, there exists two different configurations; one is a normal NS, while the other is a HS containing a quark core. These twinlike compact star solutions are called the "twin-stars" scenario [38]. The HS solution is typically more compact than the NS solution. The dashed downward cusps in Fig. 3 correspond to the unstable solutions. This is because the constant pressure in the hadron-quark matter phase transition cannot provide sufficient support against the gravity of the HS core with an increased energy density gained from the first-order phase transition. As the central density increases, the quark core can finally reach a stable state that can balance the gravitational attraction, which corresponds to the stable HS solution. The radii of twin stars with degenerate masses can be differed by several kilometers.

B. Phase transition near the crust-core interface

The crust-core transition region in the neutron star can be described as follows. The nuclear matter state in the neutron star crust is dominated by the Coulomb interactions among ions and the nuclear interaction between nucleons. Like ordinary materials, nuclear matter can also be classified to be "hard matter" and "soft matter" [7], in terms of their elastic moduli. The NS outer crust has a solid crystalline structure, which is a hard Coulomb crystal [7,58–61]. However, as the density increases, the competition between the nuclear attraction force and the Coulomb repulsive force starts to dominate the matter phase. Unlike the Coulomb force, nuclear force is typically short-range hence breaking the long-range order of the matter state. In this case, the usual spherical nuclear shapes become nonspherical complex shapes, such as lasagna or spaghetti, and the crystal structure gradually dissolves before the nuclear matter completely becomes uniform [8–11]. A typical NS has a liquid core and a solid crust, while the matter of the inner crust has ~100 meter thickness and consists of spherical nuclei, nuclei clusters, and also nuclear pastas. The liquid core has a homogeneous matter phase and therefore has a zero shear modulus, and the discontinuity interface of the shear modulus is set at the bottom of the inner crust, see Fig. 4.

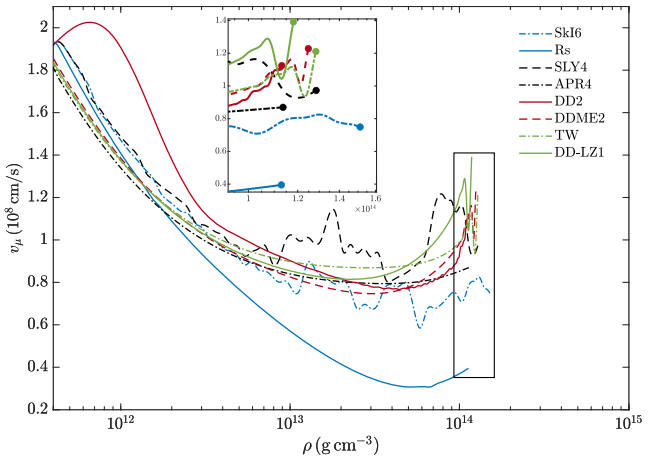

FIG. 4. Shear velocity as a function of density for different EOSs (later will be used in Table I); the EOS data is from the CompOSE database. The enlarged figure shows the shear velocity near the bottom of the inner crust.

In the fluid core, there could exist first-order phase transitions *with discontinuous density jumps* near the crust-core transition interface, as shown in Fig. 5. For example, we can construct such a phase transition at $r = r_\rho < r_\mu$ following the method presented in the Appendix of [45] based on thermodynamically consistent conditions, which means that the chemical potential μ_B on both sides of the interface are equal, while the $\partial P/\partial\mu_B$ and the density have discontinuity. An example of this first-order phase transition is presented in Fig. 6, which is based on the SLy4 nonrelativistic mean field theory model.

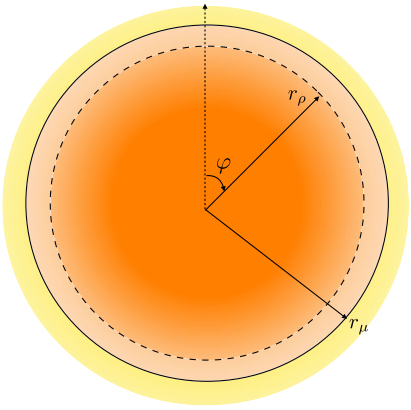

FIG. 5. The discontinuity of the density and the shear modulus can happen at different radii r_ρ and r_μ in the compact stars. The region where $r > r_\mu$ is the crust where $\mu > 0$, and the $r_\rho < r < r_\mu$ and $r < r_\mu$ regions are two fluid nuclear states with different densities. If the r_ρ is in the deeper region of the fluid core and the matter with $r < r_\rho$ is quark matter state, this compact star becomes a hybrid star. The φ denotes the azimuthal angle and the $\hat{z}$ axis is perpendicular to the paper.

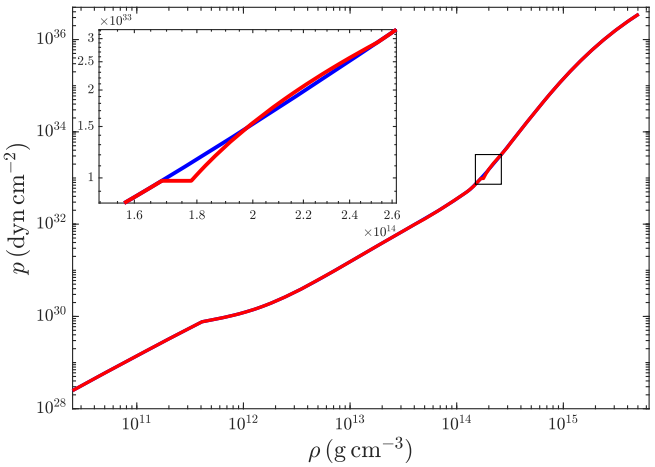

FIG. 6. Exemplary equation of state including the crust-core first-order phase transition, where the enlarged figure shows the first-order phase transition region. The blue curve is the EOS without the phase transition, which is based on the SLy4 nonrelativistic mean field theory model. The red curve is the EOS with phase transition constructed based on the SLy4 model, where the phase transition happens at $n_0 = 0.10$ fm^{-3} and the relative energy density jump is 6%.

There could be many microscopic physical mechanisms that contribute to these phase transitions, such as the emergence of the new degrees of freedom [62–66]. For example, the pion condensation can cause a transition from the normal low-density phase to the high-density phase of nuclear matter at $\rho \approx 1.3\rho_{\mathrm{sat}}$ [67]. Moreover, introducing the Δ hadron resonance in neutron stars could lead to a first-order phase transition around the crust-core transition region [63]. Bayesian inference with explicit first-order hadron-quark phase transitions from observables of canonical neutron stars shows a large likelihood (at 68% confidence level) of phase transitions at $\rho \approx 1.6^{+1.2}_{-0.4}\rho_{\mathrm{sat}}$, which is also close to the crust-core transition region [68]. In our work, with the above constructed first-order phase transition on the EOS, we want to explore whether such detail structure of the EOS can be probed by using gravitational waves, despite the microscopic mechanism.

Furthermore, by solving the TOV equation and adopting a small density jump with the emergence of a first-order phase transition, we can also obtain the corresponding M-R relation shown in Fig. 7, which means that the M-R relation is hardly affected by introducing this first-order phase transition. For the region $r > r_\mu$, that is, at the bottom of the crust, there can also be first-order phase transitions among different nuclear pasta phases. We are not interested in these phase transitions since the density jumps are often negligible [8].

As we shall see in the later sections, even with barely indistinguishable M-R relations, these phase transitions will affect the interfacial mode of the compact star, which could lead to observational signatures in the gravitational wave emitted from binary compact star systems.

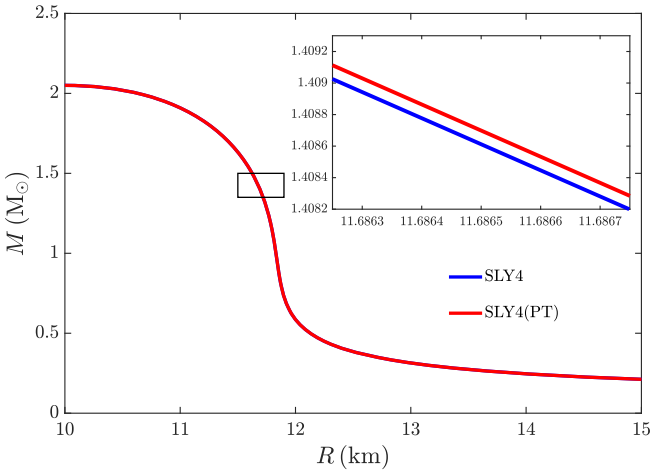

FIG. 7. Exemplary M-R relation corresponding to the EOS in Fig. 6 based on the SLy4 model with (blue)/without (red) first-order phase transition. The introduction of the phase transition does not significantly change the M-R relation, with the small difference shown in the enlarged figure. This result shows that it is difficult to probe such a phase transition (if it exists) simply by measuring the M-R relation of the compact stars.

III. INTERFACIAL MODE

A. Modes at the interfaces with shear/density discontinuity

Under the driving of external dynamical tidal force (e.g., provided by a companion star), the internal oscillation modes of a NS can be excited (e.g., the fundamental f-mode, gravity g-mode, and pressure p-mode, etc.) [35,69–71]. Among them, one type of resonant mode takes place on the interface between different matter phases called "interfacial modes" (i-mode). For example, there exists a crust-core interfacial mode [35,36,69] denoted as i_μ-mode excited at the interface between the fluid core and the solid crust, where the shear modulus μ has a discontinuous transition. For the interface where a first-order transition happens with a discontinuous density jump, there will also be another interfacial mode denoted as i_ρ-mode (sometimes named as "discontinuous-g-mode"). These modes can coexist in a NS as shown in Fig. 5.

The coupling of the i-mode and the BNS orbital motion can exchange energy between the orbital motion and the internal oscillations, thereby creating observational signatures in the gravitational waves. For example, the excitation of the crust-core interfacial mode i_μ can even induce the cracking or the melting of the NS crust [36,37,72,73]. Since the wave function and the resonant frequency of the i-mode are dependent on the EOS of a compact star, studying these physical phenomena related to the i-mode could help us understand the properties of the phases of dense matter. In the following, we will look into these interfacial modes.

The oscillation modes of the compact star can be described by the displacement of the fluid element, represented by

$$\begin{aligned}\vec{\xi}_\alpha(r,\theta,\varphi) &= \vec{\xi}_{nlm}(r,\theta,\phi)\\ &= U(r)Y_{lm}(\theta,\varphi)\hat{\mathbf{r}} + rV(r)\nabla Y_{lm}(\theta,\varphi),\end{aligned} \quad (2)$$

where $U(r)$, $V(r)$ are the displacement in the radial and tangential directions, and r is the NS radial coordinate. The properties of the interfacial mode were first studied by McDermott *et al.* in the 1980s [35,69], and the relevant astrophysical phenomena were discussed by Tsang *et al.* [36] and Pan *et al.* [37] (these modes are all i_μ-modes with discontinuous shear moduli). Following the same approach and the Cowling approximation, in this work, we calculate the interfacial mode following the Newtonian perturbation theory on a general relativity static background obtained by numerically solving the TOV equation, where the perturbative displacement of the fluid element satisfies

$$\left(\hat{\mathcal{L}} + \rho\frac{\partial^2}{\partial t^2}\right)\vec{\xi} = -\rho\nabla U_G, \quad (3)$$

in which the $\hat{\mathcal{L}}$ is a linear differential operator that describes the spatial dependence of the fluid displacement, and the "restoring force" exerts on the fluid element (for details, see [35,69] or the supplementary in [37]). The term on the right-hand side of the above equation is the tidal force exerted by the companion star's tidal gravitational potential U_G, which will be presented in Sec. IV. For solving the i-mode frequency and wave function, only homogeneous perturbation equations are needed: $(\hat{\mathcal{L}} - \rho\omega_\alpha^2)\vec{\xi}_\alpha = 0$, where ω_α is the resonant frequency of the i-mode, and $\vec{\xi}_\alpha(r) = \vec{\xi}(r)e^{i\omega_\alpha t}$ is the displacement in the rotating frame of the resonant frequency. The α denotes the $\{n,l,m\}$ quantum number that labels the eigenmodes, where n is the number of nodes of the eigenmode, l, m are the indices of the spherical harmonic function $Y_{lm}(\theta,\varphi)$. The standard shooting method [74] is applied to obtain the eigenfrequencies of the i-mode and the mode eigenfunctions are normalized as $\int d^3x|\vec{\xi}_\alpha|^2 = MR^2$. The key parameters in these perturbation equations are the $\Gamma_1 \equiv d\ln P/d\ln\rho$ and the crust shear modulus μ (which can be calculated using the formula given in Appendix B). We will introduce the two interfacial modes and their interactions in the following paragraphs.

1. Interfacial mode i_μ

Concretely, the tidal force distorts the NS core ellipsoidally in terms of $Y_{2,\pm2}(\theta,\phi)$ scalar spherical harmonics. The deformation of this core will "squeeze" the surrounding solid crust, creating a shear deformation and compression of the nuclear matter in the crust; the deformation pattern is shown in the Fig. 8(a). We have shown the wave function of the i_μ mode as the solid curves in Fig. 8(c): the wave function of the radial displacement $U(r)$ has a kink at the interface; the shear displacement $V(r)$ is hardly/significantly excited in the NS core/crust, due to the

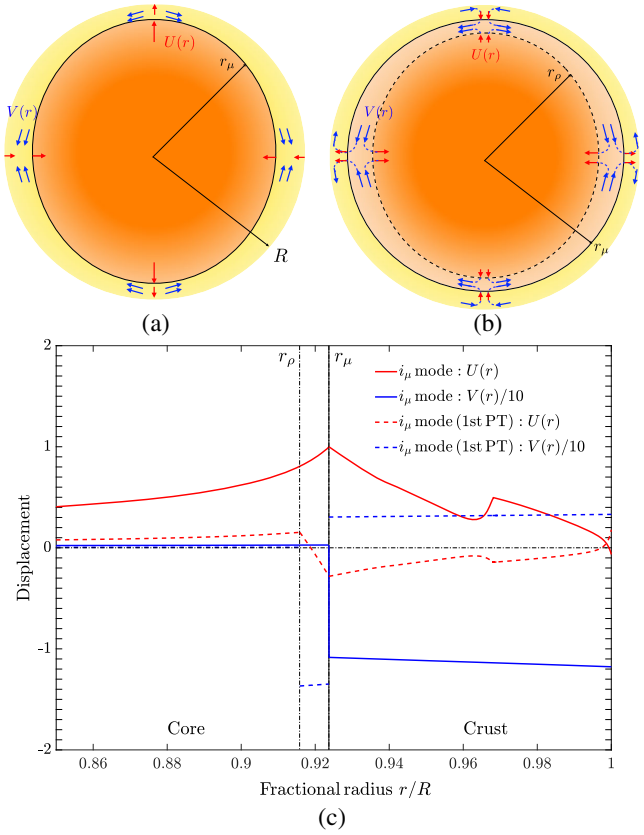

FIG. 8. Upper panel: schematic diagram showing the i_μ-mode of the compact star at the interface with shear modulus discontinuity. The (a/b) represents the deformation pattern without/with the first-order phase transition with density jump. The fluid within $r_\rho < r < r_\mu$ in (b) has zero shear modulus hence slipping freely. Lower panel: the interfacial mode wave function for the i_μ-mode based on SLy4 EOS. The red/blue solid/dashed line represents the wave functions of i_μ-mode of $U(r)/V(r)$ before/after we introduce the first-order phase transition with the density discontinuity. The vertical dashed and solid lines represent the density discontinuity interface and the shear discontinuity interface, respectively. Detailed physical explanations are presented in the main text.

discontinuity of the shear modulus crossing the crust-core interface. The directions of the shear motion of the fluid/solid element of the two sides of the interface are opposite to each other.

With the introduction of the first-order phase transition at r_ρ, the interfacial mode i_μ is changed with the deformation pattern shown in Fig. 8(b). It is important to note that the fluid within $r_\rho < r < r_\mu$ has zero shear moduli and can slip freely. This means that the free-slipping fluid layer within $r_\rho < r < r_\mu$ will share the displacement of the crust bottom. Under the tidal deformation with the $Y_{22}(\theta, \varphi)$-pattern at $\varphi = \pi/2$, the shear motion of the free-slipping fluid element will meet and combine to push the core inwardly and the crust outwardly. Therefore, the wave function $U(r)$ for the i_μ mode in Fig. 8(c) changes its sign when crossing the $r_\rho < r < r_\mu$ region. For the shear wave function $V(r)$, it is also easy to see that $V(r)$ changes its sign when crossing the two interfaces. The shear displacement is relatively large within $r_\rho < r < r_\mu$ compared to the shear motion in the core and the crust because the fluid element between the two interfaces is freely slipping during the oscillation.

The i_μ-mode is typically soft and has a frequency around 50 Hz, see Table I for different EOSs. Its frequency will further decrease when interacting with the i_ρ-mode, as we shall discuss later.

2. Interfacial mode i_ρ

For a fluid compact star where the shear modulus vanishes everywhere, there exists an oscillation mode i_ρ excited at the density discontinuity interface, with the typical deformation pattern shown in Fig. 9(a) and wave function shown as solid lines in Fig. 9(c). Introducing the shear-modulus discontinuity (or the NS crust) will modify the original "bare" i_ρ-mode to that shown in Fig. 9(b) and the dashed lines in Fig. 9(c). The wave functions here are different from the i_μ-mode case, where the radial displacement $U(r)$ does not flip the sign crossing the transition region $r_\rho < r < r_\mu$, and the shear displacement $V(r)$ only flips its sign when crossing the shear discontinuity interface. The physical picture of the i_ρ-mode can be understood as both the crust and the $r_\rho < r < r_\mu$ fluid that are passively displaced under the driving of the core deformation in $r < r_\rho$. However, in the case of the i_μ-mode, it is the crust and the $r < r_\rho$ core passively displaced under the driving of the slipping of the fluid in $r_\rho < r < r_\mu$. Such a difference is the key to distinguishing the deformation pattern between the i_μ-mode and i_ρ-mode.

The i_ρ-mode is relatively hard with a typical frequency larger than 100 Hz, see Table I for the results for different EOSs based on different nuclear physics models. The interaction with the i_μ-mode will increase the frequency of the i_ρ-mode.

Furthermore, it is worth noticing that this interfacial mode i_ρ is actually the Kelvin-Helmholtz wave (KH wave) in fluid dynamics. Kelvin-Helmholtz wave is the wave excited at the interface of two fluids with different densities in a gravitational field, which exactly corresponds to the i_ρ-mode here (we do not expand the discussions on the Kelvin-Helmholtz wave theory, for which we refer to the textbooks [75]). The relationship of the frequency of the KH waves and the densities when the fluid bulk velocity is zero is: $\omega \propto \sqrt{(\rho_- - \rho_+)/(\rho_- + \rho_+)}$, where the ρ_- and ρ_+ are the densities of the fluids at inner and outer sides of the interface. In the i_ρ-mode case, for the SLy4 EOS in Table I, the phase transition width $\Delta\rho = \rho_- - \rho_+$ is around ~5%. This value is in Fig. 5 and is chosen to be 1.5%–2.0%, while the $\rho_- + \rho_+$ is about the same. Therefore, it is

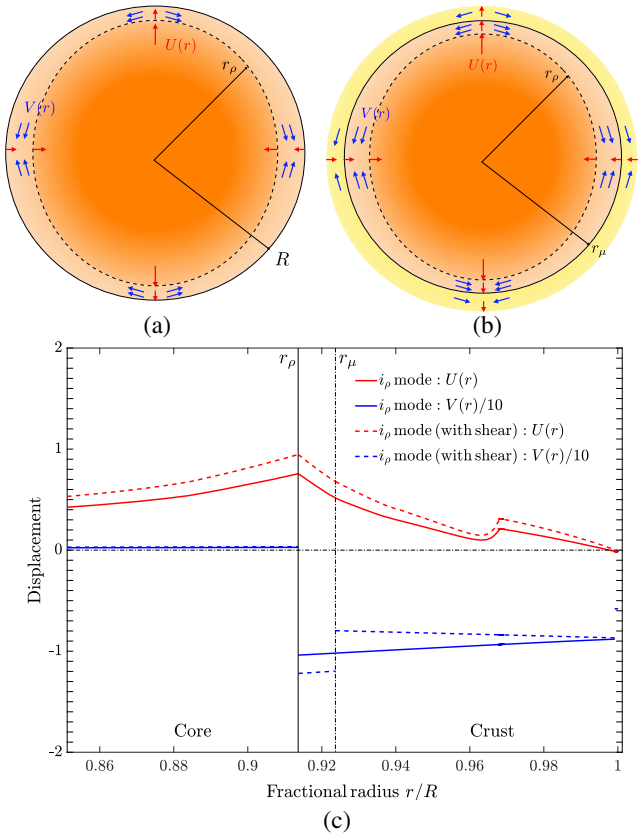

FIG. 9. Upper panel: schematic diagram showing the i_ρ-mode of the compact star at the interface with density discontinuity. The (a/b) represents the deformation pattern without/with the shear modulus transition. The fluid within $r_\rho < r < r_\mu$ in the right panel has zero shear moduli thereby slipping freely. Lower panel: the interfacial mode wave function for the i_ρ-mode based on SLy4 EOS. The red/blue solid/dashed line represents the wave functions of i_ρ-mode of $U(r)/V(r)$ before/after we introduce the shear modulus transition. The vertical dashed and solid lines represent the shear discontinuity interface and the density discontinuity interface, respectively. Detailed physical explanations are presented in the main text.

reasonable to expect that there will be a difference of the frequencies by a factor around 1.6–2.0.

3. Mode interactions

In the above analysis, we showed that the $i_{\mu/\rho}$-mode frequencies and wave functions will be altered when both density and shear discontinuity interfaces exist. This phenomenon can be qualitatively understood as the mode-mode interaction, in terms of the following simple Hamiltonian:

$$\mathcal{H} = (\xi_\mu, \xi_\rho)\begin{pmatrix} \omega_\mu & \chi \\ \chi & \omega_\rho \end{pmatrix}\begin{pmatrix} \xi_\mu \\ \xi_\rho \end{pmatrix}, \tag{4}$$

where the $\omega_{\mu/\rho}$ is the frequency of $i_{\mu/\rho}$ mode when only shear-modulus/density discontinuity interface exists. The χ phenomenologically describes their interactions, which depends on the radial distance between these interfaces. Typically, for a first-order phase transition that does not significantly alter the M-R relation; this distance cannot be too large. Therefore, the excitation of $i_{\mu/\rho}$ mode must simultaneously drive the $i_{\rho/\mu}$-mode since their wave functions are significantly overlapped. In this case, we will have an avoid-crossing effect for the mode-mode interaction, that is, the new eigenfrequencies become

$$\tilde{\omega}_\rho = \frac{1}{2}\left[\omega_\mu + \omega_\rho + \sqrt{(\omega_\mu - \omega_\rho)^2 + 4\chi^2}\right] > \omega_\rho,$$
$$\tilde{\omega}_\mu = \frac{1}{2}\left[\omega_\mu + \omega_\rho - \sqrt{(\omega_\mu - \omega_\rho)^2 + 4\chi^2}\right] < \omega_\mu, \tag{5}$$

which are manifested in Table I. In obtaining Table I, we first compute the interfacial modes i_μ or i_ρ when there is only shear-modulus discontinuity or density discontinuity, respectively. After that, we find the eigenfrequencies corresponding to these two modes when both discontinuity interfaces coexist. Physically, the introduction of the free slipping layer effectively shares the excitation of the core in i_μ-mode, causing its eigenfrequency to decrease. During the excitation of the i_ρ-mode, the introduction of shear modulus in the crust makes it harder for the core to drive the $r > r_\rho$ part of the compact star thereby increasing the mode frequency.

One specific case is when the two interfaces coincide, where the free-slipping fluid in the $r_\rho < r < r_\mu$ region vanishes and the two modes merge into one mode denoted as $i_{\mu\rho}$-mode, with frequencies shown in Fig. 10. In the limiting case of $r_\rho = r_\mu$, the intermediate layer of fluid disappears and so does the i_μ-mode associated with this intermediate fluid layer. This can be seen from Fig. 8(b) that the fluid element motion vanishes at $\varphi = 0, \pm\pi/2, \pi$ in this limiting case. Moreover, the $l = 2$ harmonic function $Y_{2,\pm=2}(\theta, \varphi) \propto \cos 2\varphi$ also vanishes at $\varphi = \pm\pi/4, \pm 3\pi/4$. Then there exists totally eight nodes when $r_\rho = r_\mu$, which means that this mode is no longer the $l = 2$ mode even if the fluid motion got excited and thereby cannot be excited by the orbital motion at the leading order.

Therefore, in a binary compact star system, it becomes relatively more difficult for the orbit motion to drive the interface oscillation $i_{\mu\rho}$ when the shear modulus discontinuity happens at the same radius as the density discontinuity, compared to the driving of the i_μ. For the unified relativistic mean field EOSs in the CompOSE database [76–78] FSU2R, FSU2H, and TM1e [79], which have relatively soft inner crust structures, we find that these unified EOSs have the two interfaces coincide. In these EOSs, the crusts are connected to the core with an abrupt energy jump and a pressure plateau (i.e., a first-order phase transition). The connection happens at a density where the heavy nuclear clusters dissolve with a shear-modulus discontinuity. The relative energy density jumps are

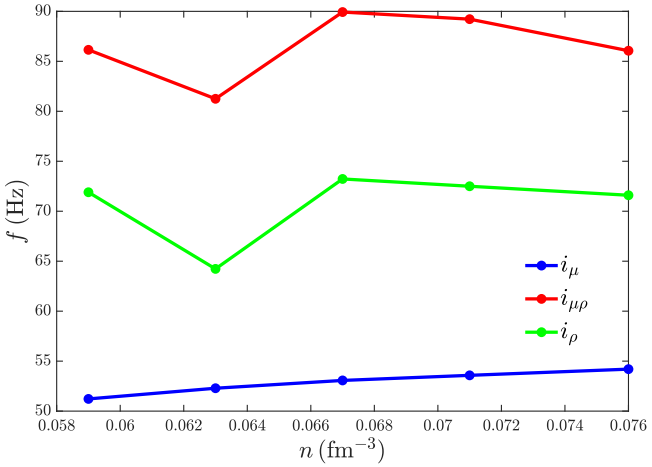

FIG. 10. The interfacial mode when the two interfaces coincide (using SLY4 EOS as an example): $r_\mu = r_\rho$, which we denote as the interfacial mode $i_{\mu\rho}$. In this case the fluid region $r_\rho < r < r_\mu$ vanishes, and the soft mode shown in Fig. 8(b) disappears. The horizontal axis is the number density n at which the shear modulus happens accompanied with the density jump, which serves as a free parameter due to its uncertainty. The blue/green dots are the $i_{\mu/\rho}$ frequencies when we consider the effects of the shear-modulus/density discontinuity at density n, respectively. The density discontinuity constructed here is rather small, ranging from 1.5% to 2.0%. It is shown that shifting n has a minor influence on the i_μ mode frequency, while the introduction of the density discontinuity will significantly increase the mode frequency.

16.4%, 15.4%, and 14.2% with the number density of the bottom of the crust being 0.083 fm^{-3}, 0.087 fm^{-3}, and 0.089 fm^{-3} for the FSU2R, FSU2H, and TM1e, respectively. Accordingly, the $i_{\mu\rho}$-mode frequencies of $1.4M_\odot$ are 176.6 Hz, 177.2 Hz, and 187.4 Hz. This demonstrates that these unified EOSs in the CompOSE database with coinciding interfaces only have one $i_{\mu\rho}$ interfacial mode with a higher frequency around 180 Hz.

B. Interfacial modes affected by the quark core

Besides the phase transition, which happens near the crust-core transition region, we have also investigated the strong interaction phase transition, which leads to the existence of quark matter in the core of a HS. Lau *et al.* [34] analyzed the interfacial mode excited at the interface between the crystalline quark matter core and a fluid hadronic envelope, which has a relatively high frequency ranging from 300 Hz to 1500 Hz. Intuitively, even if the quark core is not crystalline but a fluid core, then there could also exist an interfacial mode (similar to the i_ρ-mode discussed in the previous section) at the interface of the first-order hadron-quark phase transition. Although this interface is in the relatively deeper region of the fluid core, it can still affect the properties of the interfacial mode excited at the crust-core interface with shear-modulus discontinuity.

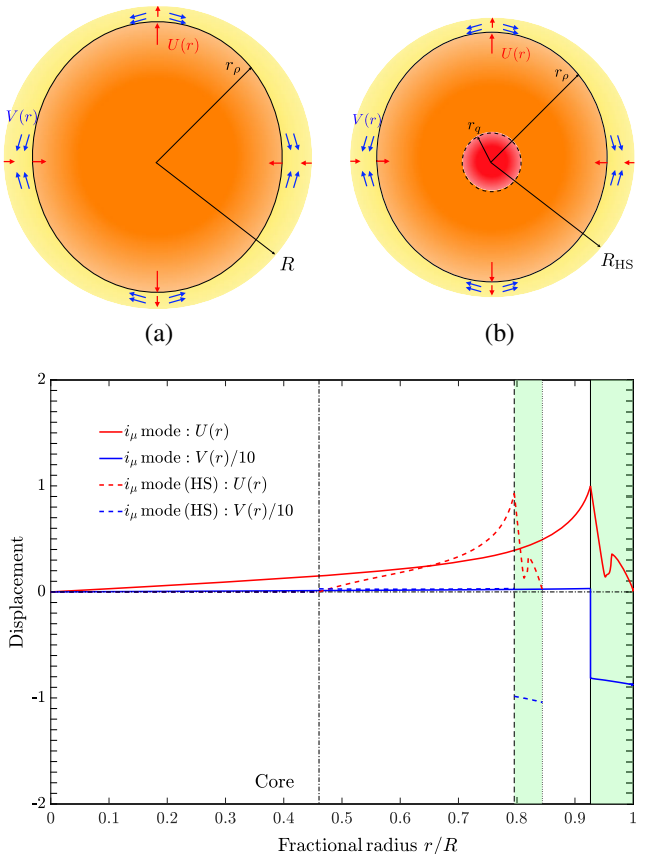

FIG. 11. Upper panel: schematic diagram showing the i_μ-mode of the compact star (HS and NS with the same mass $1.6M_\odot$) at the interface with the shear modulus discontinuity. The (a/b) represents the deformation pattern without/with the hadron-quark first-order transition. For the compact star with the same mass, the radius of a NS is typically larger than that of a HS, and these two configurations are called twin stars. Lower panel: the interfacial mode wave function for the i_μ-mode based on SLy4 EOS. The red/blue solid/dashed line represents the wave functions of the i_μ-mode of $U(r)/V(r)$ before/after we introduce the hadron-quark transition. The vertical dash-dotted and dashed lines represent the hadron-quark interface and the shear discontinuity interface for the HS, respectively. The solid vertical line and the dotted vertical line are the shear discontinuity interface for the NS and the surface of the HS, respectively. The R is the radius of the NS and the green-shaded region is the crust of the NS/HS.

As we mentioned in the previous section, the NS and HS with the same mass but different radii are called twin stars. Interfacial modes may help us distinguish the twin branch, of which the wave functions are shown in Fig. 11 and the frequency differences are shown in Fig. 12, where we take the CSS model with the speed of sound $c_{\rm QM} = c$ for the quark core. We plot the frequency of the i_μ-mode for seven different twin-star solutions (i.e., the NS and HS with the same mass) corresponding to seven different hadron-quark transition densities where NL3 hadronic EOS transits to CSS quark EOS.

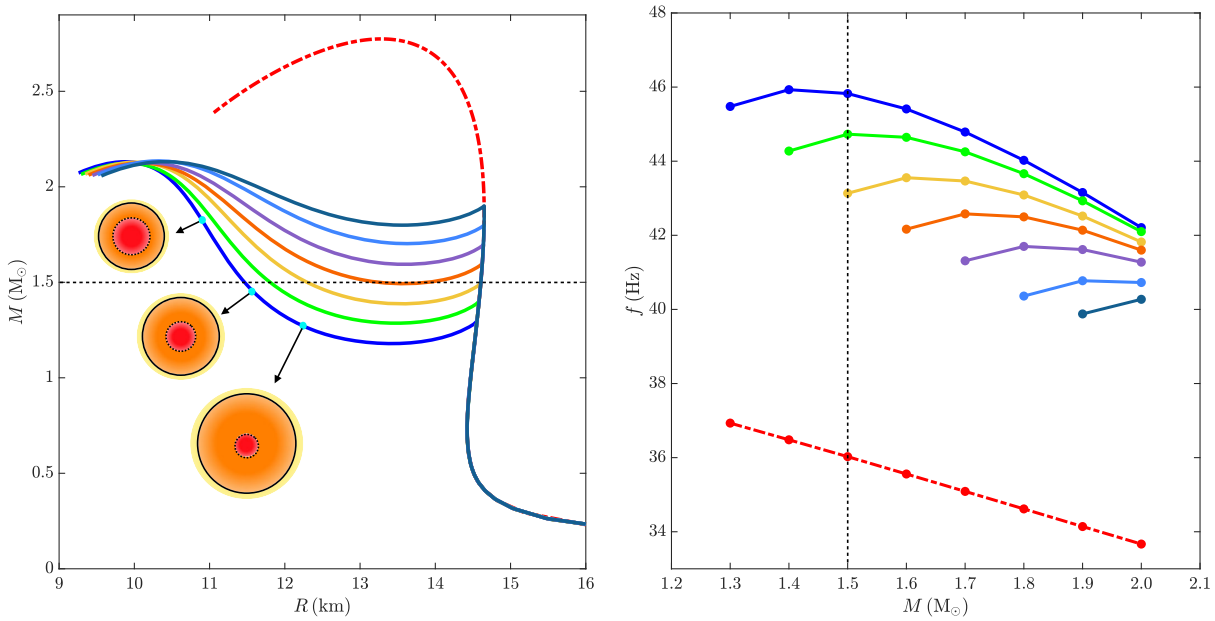

FIG. 12. The interfacial mode frequency affected by the quark core. Left panel: twin star M-R relations constructed using different hadron-quark transition densities. To explore the upper limit of the twin-star's effects, the speed of sound of the quark EOS is assumed to be c (which means a very stiff quark matter), and the relative energy density jump $\Delta\rho/\rho_{\rm trans}$ is as large as possible until reaching the observational constraints $M_{\rm max} \approx 2.1 M_\odot$. Right panel: the red dashed line represents the frequency of the i_μ-mode at the NS branch (the solutions with larger radii) for different masses, and the solid line corresponds to the HS branch (the solutions with smaller radii) for different masses. The two frequencies of the two solutions in a twin-star EOS are typically differed by ∼7–10 Hz. The EOSs of the quark core and the nuclear matter are the CSS model and NL3 model, respectively. Detailed physical explanations are presented in the main text.

For one particular hybrid star EOS, the frequency first increases and then decreases as the mass of the compact star increases. The initial frequency increase is due to the reason that, for the stable HS branch of the EOS where $dM/dR < 0$, the HS radius R first decreases rapidly as M increases. Moreover, there also exists an interfacial mode at the hadron-quark phase transition interface discussed by Lau *et al.* [34], which can also induce an avoid-crossing effect with the crust-core interfacial mode. As the mass further increases and the radius further decreases, the relative distance between the nuclear-quark phase transition interface and the crust-core interface shrinks, which creates a larger overlap between these two interfacial modes thereby a stronger avoid-crossing effect, see Fig. 12. This is why the frequency then decreases after reaching a peak value. For one particular compact star mass (e.g., the horizontal dashed line shown in the left panel of Fig. 12), different EOSs lead to different radii of the HS, hence also different i_μ-mode frequencies shown in the right panel of Fig. 12.

IV. GRAVITATIONAL WAVE SIGNATURE

A. Interfacial mode couples to the orbital motion

The excitation of the crust-core i-mode by the tidal force in a binary compact star system (see Fig. 13) will convert part of the energy of the orbital motion to the NS oscillation, thereby affecting the waveform of the gravitational waves. This phenomenon is called the dynamical tidal coupling. The internal oscillation of a NS can have many different modes, such as the pressure mode, fundamental mode, gravity mode, Rossby wave, and interfacial mode. The frequencies of the pressure mode and fundamental mode are usually above the binary inspiral frequency, while the gravity mode cannot efficiently couple to the orbital tidal. The Rossby wave also couples weakly since it is driven by the relativistic gravitomagnetic effect [80,81]. The crust-core interfacial mode has a relatively lower frequency and a larger coupling to the tidal field. Therefore, the interfacial mode is of particular interest that may leave signatures in the GW emitted from the inspiral stage of a binary compact star system, and hence could be used as a probe of NS EOS and internal structures. In this section, we discuss the impact of nuclear matter phase transitions on the GW signals emitted from the binary systems.

Our analysis of the tidal excitation of the i-mode follows the standard method presented in [37,82]. For the comprehensive purpose, we summarize the basic procedure as follows. The tidal excitation of the i-mode can be described by a driven harmonic equation:

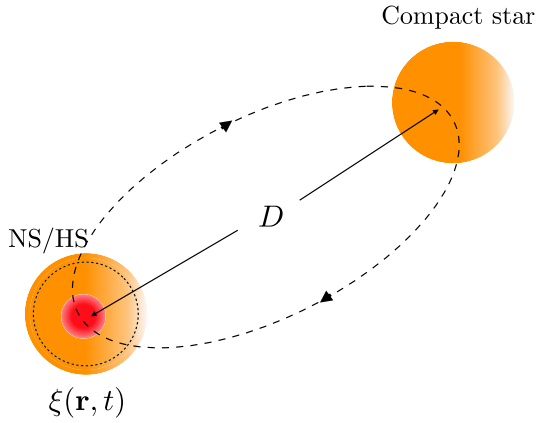

FIG. 13. Binary compact stars system. The orbital motion of the binary system will exchange energy with the internal oscillation of the NS/HS through the tidal excitations. The companion compact star can be a NS, HS, or even a black hole. In this case, the interfacial mode will affect the gravitational waves emitted from the binary system.

$$\ddot{a}_m(t) + \omega_m^2 a_m(t) + \gamma \dot{a}_m(t) = \frac{GM_* W_{2m} Q_{2m}}{D^3(t)} e^{-im\Phi(t)}. \quad (6)$$

In this formula, the a_m are the mode expansion coefficients defined as $\xi(\mathbf{r},t) = \sum_m a_m(t)\xi_m(\mathbf{r})$, where m denotes the azimuthal quantum number of the eigenmode with angular pattern $Y_{2m}(\theta,\varphi)$, and the $\xi_m(\mathbf{r})$ is the neutron star eigenmode functions. The right-hand side is the tidal force derived from the tidal potential

$$U_G = -GM_* \sum_{l,m} W_{lm} \frac{r^l}{D^{l+1}} e^{-im\Phi(t)} Y_{lm}(\theta,\phi), \quad (7)$$

where the W_{lm} is the spherical harmonics expansion parameter, M_* is the mass of the companion star, D is the orbital distance between the two NSs, and the $\Phi(t)$ is the orbital phase. The spherical coordinate (r,θ,ϕ) describes the position of the fluid element in the tidally deformed NS. The Q_{lm} is the tidal coupling coefficient, that is, the overlap between the compact star's internal Y_{lm}-oscillation mode and the external tidal force, given by (for $n=1$, $l=2$)

$$Q_{2m} = Q_{2m}^U + Q_{2m}^V = \frac{1}{MR^2}\int d^3x \rho \vec{\xi}^*_{2m} \cdot \nabla(r^2 Y_{2m}) = \frac{2}{MR^2}\int_0^R \rho r^3 dr[U(r) + 3V(r)]. \quad (8)$$

It is important to note that the Q_{2m} coefficients are different for different modes, which we listed in Table II. This result can be understood using the wave function modified by the phase transition is shown in Fig. 8(c)and Fig. 9(c). For example, the tidal coupling coefficient of the radial deformation $U(r)$ of the i_μ-mode drops significantly when we introduce the first-order phase transition at r_ρ because the integrand $U(r)$ flips its sign when crossing the region $r_\rho < r < r_\mu$.

TABLE II. Exemplary tidal coupling coefficient Q_{22} of EOS DD-LZ1 affected by first-order phase transition.

Mode	Q_{22}	Q_{22}^U	Q_{22}^V
i_μ	0.0285	0.0425	−0.0140
i_ρ	−0.0173	0.0354	−0.0527
i_μ (1st PT)	−0.0230	0.0001	−0.0231
i_ρ (with shear)	0.0090	0.0437	−0.0347

The γ parameter is the dissipation rate of the i-mode, which depends on the microscopic details, and was phenomenologically discussed in [37,82]. It is worth noting that the tidal coupling to the interfacial mode could lead to some nonelastic effects. For example, Tsang *et al.* showed that when the shear motion of the crust reaches its elastic limit a resonant shattering of the NS crust will happen [36,73], which could be a possible reason for the precursor of the short gamma-ray burst [36]. Moreover, Pan *et al.* recently considered the tidal heating and the melting of the NS crust due to the excitation and dissipation of the crust-core interfacial mode, and they studied its possible signatures in the GW observations. In this case, the ω_α is a time-dependent resonant frequency of the i-mode since the elastic modulus of the NS crust can decrease with an increasing temperature, and the dissipation rate γ can also be time dependent. Since the crust cracking/melting process depends on the details of nuclear matter, we only qualitatively discuss these nonelastic effects in this work for an illustrative purpose later.

In computing the tidal driving on the right-hand side of Eq. (6), we use the no-backaction approximation discussed and justified in [80] so that the variation of the distance $D(t)$ and phase satisfies

$$\dot{D} = -\frac{64G^3}{5c^5}\frac{MM_*(M+M_*)}{D^3}, \qquad \dot{\Phi} = \sqrt{\frac{G(M+M_*)}{D^3}}, \quad (9)$$

which assumes that the evolution of the orbital distance is assumed to be dominated by gravitational wave radiation. When the orbital motion is on-resonance with an internal mode frequency, a tidal resonance happens. For the NS with only shear-modulus/density discontinuity in the crust-core transition region as in Figs. 8(a) and 9(a), the tidal force of the inspiral stage will excite one resonance at $f_{i_{\mu/\rho}}$, of which the values are distinct from each other. For the NS with both shear-modulus and density discontinuity in the crust-core transition region as in Figs. 8(b)and 9(b), there will be two resonances successively excited at different

frequencies $f_{\tilde{i}_{\mu/\rho}}$ during one inspiral process. These tidal resonances will affect the gravitational wave signal and provides a way to probe the nuclear phase transition in compact stars.

B. GW waveform and the detectability

1. Full elastic case

First, we discuss the situation where there is no inelastic process in the neutron star oscillation. The effect on the orbital cycle and hence the phase of the gravitational wave radiated by the inspiraling BNS has been studied by Lai [80,82], where the phase shift is generally given by

$$\Delta\phi_{j\,\mathrm{GW}} = 2\pi\omega_{\mathrm{orb}}\Delta E/\dot{E}_{\mathrm{tot}}, \tag{10}$$

in which ω_{orb} is the orbital frequency on resonance with the interfacial mode, $\dot{E}_{\mathrm{tot}}$ is the energy loss rate of the entire BNS system (consists of orbital energy and the NS energy and typically equal to the emission power of the gravitational waves), and ΔE is the change of the NS energy. In the case of no crust melting or shattering, the ΔE is the energy stored in the NS oscillation mode and the corresponding phase shift can be written as follows [82]:

$$\begin{aligned}\Delta\phi_{j\mathrm{GW}} &= -\frac{5\pi^2}{1024}\left(\frac{Rc^2}{GM}\right)^5\frac{2q}{1+q}|Q^j_{2,2}|^2(2\pi\tilde{f}_j)^{-2}\\ &\approx 54\left(\frac{100\ \mathrm{Hz}}{f_j}\right)^2\left(\frac{Q^j_{2,2}}{0.03}\right)^2\left(\frac{1.4M_\odot}{M}\right)^4\\ &\quad\times\left(\frac{R}{10\ \mathrm{km}}\right)^2\frac{2q}{1+q},\end{aligned} \tag{11}$$

where $q\approx 1$ is the mass ratio, and $\tilde{f}_j = f_j\sqrt{R^3/M}$ is the normalized dimensionless i-mode frequency. In obtaining the above formula, we have considered the fact that there are two $m=\pm 2$ excited modes. Simple estimations can show that the phase shift induced by the tidal excitation of the interfacial mode is quite large compared to the g-mode or f-mode if the excitation process is entirely elastic. If there exists an inelastic process, such as crust melting, the phase shift would be much smaller as analyzed in [37] since the crust will melt before the resonant oscillation develops.

When the time-varying tidal force sweeps through the resonant frequencies, there will be a modification to the gravitational wave phase represented by

$$\Delta\Phi(f) = -\sum_j\sum_{A=1,2}\delta\phi^{(A)}_{\mathrm{jGW}}\left(1-\frac{f}{f^{(A)}_j}\right)\Theta(f-f^{(A)}_j), \tag{12}$$

compared to the phase $\Phi(f)$ in the GW waveform (in the frequency domain) without this tidal resonance effect,

$$h(f) = \tilde{A}(f)\exp[i\Phi(f)], \tag{13}$$

where $\tilde{A}(f)$ and $\Phi(f)$ are the gravitational wave strain amplitude and phase in the frequency domain. Here the summation over $A=1,2$ takes into account the oscillation mode of two compact stars in a binary system, and the summation over j accounts for the situation where there will be more than one resonant mode to be excited. For example, when the shear and density discontinuity coexists in a NS, there will be two internal modes that will be excited successively. In this case, there will be eight new parameters: $\delta\phi^{(1,2)}_{i_{\mu/\rho}}$ and $f^{(1,2)}_{i_{\mu/\rho}}$ enter into the GW waveform. For the binary system consisting of two similar compact stars, their internal modes have similar structures and properties, that is $f^{(1)}_i \approx f^{(2)}_i$, which gives the possibility to reduce the number of parameters of this model as raised in [37]:

$$\Delta\Phi(f) \approx -\sum_j\delta\bar{\phi}_{\mathrm{jGW}}\left(1-\frac{f}{\bar{f}_j}\right)\Theta(f-\bar{f}_j), \tag{14}$$

where we define $\delta\bar{\phi}_{j\,\mathrm{GW}} = \sum_A\delta\phi^{(A)}_{j\mathrm{GW}}$ and $\bar{f}_j = \delta\bar{\phi}_{j\mathrm{GW}}/(\sum_A\delta\phi^{(A)}_{j\mathrm{GW}}/f^{(A)}_j)$. For the compact star with two resonant modes excited, there will be only four new parameters under this approximation. The point particle waveforms used in this work also follows [34], where we use IMRPhenomD template with 5th Post-Newtonian (PN) and 6th PN tidal contributions and cut-off frequency chosen as the innermost stable circular orbit frequency (for details, see [34]). When using these waveform templates, we recomputed the tidal deformability using the EOS modified by the phase transition is shown in Table III.

We model the detectability using the Fisher information matrix as in [34,83,84], supposing that the gravitational wave signal is strong enough to have a high signal-to-noise ratio, and the detector noise is Gaussian. The effective Fisher matrix incorporating *a priori* information following [83] with template parameters $\{\theta_m\}$ defined by

TABLE III. The tidal deformability of different EOSs with $1.4M_\odot$. This table shows that the introduction of the first-order phase transition at r_ρ only induces a slight change of the tidal deformability. The tidal deformability coefficient in the template waveform is $\tilde{\Lambda}$, which is a weighted combination of the tidal deformability of the two stars in a BNS system. When $M_1 = M_2$, we have $\tilde{\Lambda} = \Lambda_1 = \Lambda_2$. The detection uncertainty calculated from Fisher information is $\Delta\tilde{\Lambda}\sim 100$, based on *Cosmic Explorer* sensitivity. This means that the tidal deformability can not be used to probe the first-order phase transition at r_ρ.

EOS	SKI6	RS	SLY4	APR4	DD2	DDME2	TW	DD-LZ1
Λ	488	597	299	248	682	712	406	722
Λ_{PT}	496	651	303	260	714	738	424	755

$$\tilde{\Gamma}_{mn} = \left(\frac{\partial h}{\partial\theta_m}\middle|\frac{\partial h}{\partial\theta_n}\right) + \frac{\delta_{mn}}{\sigma^2_{m\text{prior}}}, \tag{15}$$

where the inner product $(a|b)$ is defined as

$$(a|b) = 2\int_0^\infty \frac{a^*(f)b(f) + a(f)b^*(f)}{S_{hh}(f)}, \tag{16}$$

with $S_{hh}(f)$ is the strain noise spectral density of the GW detector. The root-means-square (rms) for estimating the parameter θ_m now can be written as follows:

$$\Delta\theta_m = \sqrt{(\tilde{\mathbf{\Gamma}}^{-1})_{mm}}, \tag{17}$$

where $\tilde{\Gamma}^{-1}$ is the inverse of the effective Fisher information matrix. The phase shift is detectable if it is larger than the error for measuring the parameter $\theta_m = \delta\bar{\phi}_{j\text{GW}}$: $\Delta\delta\bar{\phi}_{j\text{GW}}$. In Fig. 14, we plot the detectability of the interfacial modes computed using different EOSs, based on the designed sensitivity of advanced Laser Interferometer Gravitational Wave Observatory (LIGO) [85] and the third generation detector *Cosmic Explorer* [86]. For the i_μ-mode at the shear discontinuity interface with lower frequency, there is a significant detectability of these modes from the GW observations if the excitation process is entirely elastic; while the interfacial mode at the density discontinuity interface is relatively more difficult to be detected due to its high frequency. The introduction of the first-order transition reduced the frequency of the i_μ-mode while increasing its detectability.

2. Influence of the inelasticity to the detectability

The results presented in Fig. 14 show that for the elastic deformation there is a significantly high detectability. However, as we mentioned before, Tsang *et al.* and Pan *et al.* [36,37] investigated the possible inelastic process that happens in the deformation of a NS crust. In particular, Pan *et al.* [36,37] considering the melting of the crust and the basic physical process describe it as follows: the tidal interaction drives the i-mode so that the shear motion may exceed the crust yield limit and the plastic deformation starts, accompanied with the mode energy converting into the thermal energy. Gradually, accumulating heating energy will start to melt the crust, and it takes ~20 orbit periods to completely melt down the crust which costs about 10^{47} ergs energy. Pan *et al.* [36,37] gave the formula for estimating the phase correction induced by the crust melting as

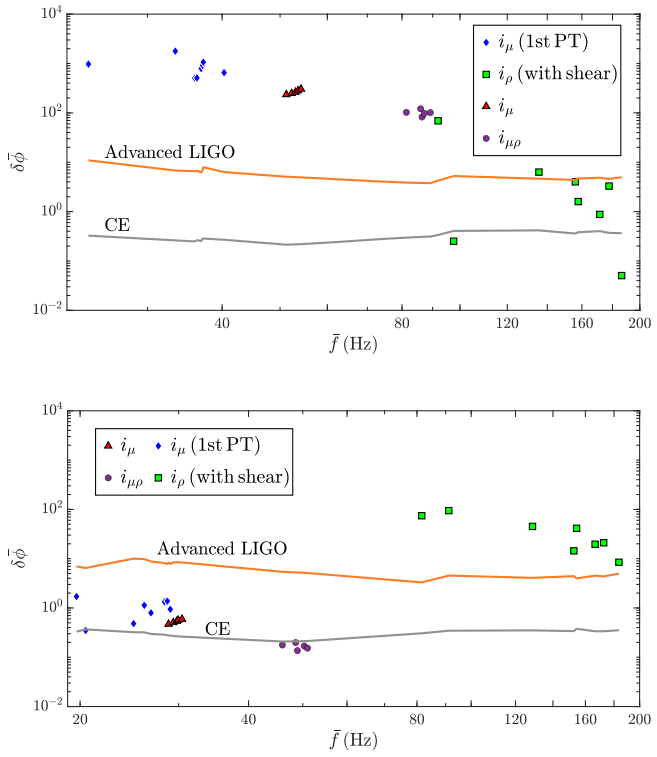

FIG. 14. Upper panel: detectability of the interfacial modes for the elastic NS deformations. The vertical axis is the phase shift $\delta\phi$ due to the coupling of the orbit motion and the interfacial mode, and the horizontal axis is the redefined interfacial mode frequency for the binary system [see the text below Eq. (14)]. The yellow and grey lines are the detectability threshold of advanced LIGO (using its designed sensitivity) and the proposed *Cosmic Explorer*, which are obtained using the Fisher information analysis. The blue diamond points and the green squared points describe the phase induced by the interfacial modes shown in Fig. 8(b) and Fig. 9(b), which are affected by the mode mixing. The red triangle points and circular purple points represent the interfacial modes i_μ without the effect of the density discontinuity shown in Fig. 8(a) and the situation when the shear and density discontinuity merges, respectively. We calculate the detectabilities for eight different EOSs in Table I, and the mode with lower frequencies is easier to be detected. Lower panel: detectability of the interfacial modes when the crust-melting process is introduced; the setting of the figure is the same as that of the upper panel.

$$\begin{aligned}\delta\phi_{\text{melt}} &= \frac{2\omega_{\text{orb}}E_{\text{melt}}}{P_{\text{GW}}} \\ &\approx \frac{0.18}{q^2}\left(\frac{1+q}{2}\right)^{2/3}\frac{E_{\text{melt}}}{10^{47}\text{ erg}}\left(\frac{M}{1.4M_\odot}\right)^{-10/3} \\ &\quad\times\left(\frac{f_{\text{GW,melt}}}{100\text{ Hz}}\right)^{-7/3},\end{aligned} \tag{18}$$

which can be used to estimate the effective melting to the detectability. Using the approach as in Pan [37], we plot the effect of melting on the detectability of interfacial modes for different EOS models in the lower panel of Fig. 14, where we

considered the temperature-dependent shear modulus and the detailed crust heating model (summarized in the Appendix for illustrative purposes). The results in Fig. 14 can be understood as follows: (1) The effects on the GW phase due to the coupling of the orbital motion with the i_μ modes become more difficult to observe since the melting destroys the crust, and the melting energy $E_{\rm melt}$ is only a small fraction compared to the resonant energy when the i_μ-mode is fully swept through during resonance. (2) The resonant frequency for the driving of the crust-core interfacial modes i_μ systematically move leftward because the heating softens the crust matter. Moreover, since the exceeding of elastic deformation happens before the original resonant point, the accumulation of heat and the meltdown of the crust effectively lower the resonant frequencies, which is beneficial to the observability of the $i_{\mu\rho}$ mode (see Fig. 14). (3) The melting effect will convert the crust from a Coulomb crystal to a Coulomb liquid, so that the discontinuity of the shear modulus that exists in the cold NS diminishes. Therefore, the corresponding interfacial mode i_μ also disappears. Hence, the coupling between the i_μ and i_ρ also diminishes, which will create a decrease of the i_ρ frequency and an increase of the tidal coupling coefficient Q_{2m} (see Table II) of the i_ρ frequency. This will increase the signal of the coupling between orbital motion and the interfacial mode i_ρ and also its detectability compared to the elastic case.

C. Distinguishing the twin star

The above discussions focus on probing the nuclear phase transition near the surface of the neutron fluid core. Now we discuss the possibility of using the interfacial mode to probe the nuclear-quark phase transition.

As mentioned in Sec. III B, the i_μ-mode frequencies of NSs and HSs differ up to 7–10 Hz. In reality, the resonance excitation does not happen instantaneously at the resonant orbital frequency. Following [82], the total number of orbital cycles that the binary system evolves during the period of the effective resonant excitation of the i_μ-mode is

$$\delta N_{{\rm orb},i} \approx 12\left(\frac{f_i}{100\ {\rm Hz}}\right)^{-5/6}\left(\frac{M}{1.4M_\odot}\right)^{-5/6} q^{-1/2}\left(\frac{2}{1+q}\right)^{1/6}, \tag{19}$$

which means that there is a bandwidth of orbital frequency experienced during the resonant excitation. If the internal oscillation frequency of the NS in a NS-NS binary system is different from that of the HS in a HS-NS binary system with the same mass by δf_i, and δf_i is smaller than the bandwidth of the resonant excitation, then this frequency difference is not resolvable and thereby difficult to distinguish the twin-star component.

This can be formulated in another equivalent way. The number of cycles for the BNS evolving from f_1 to f_2 can be obtained by

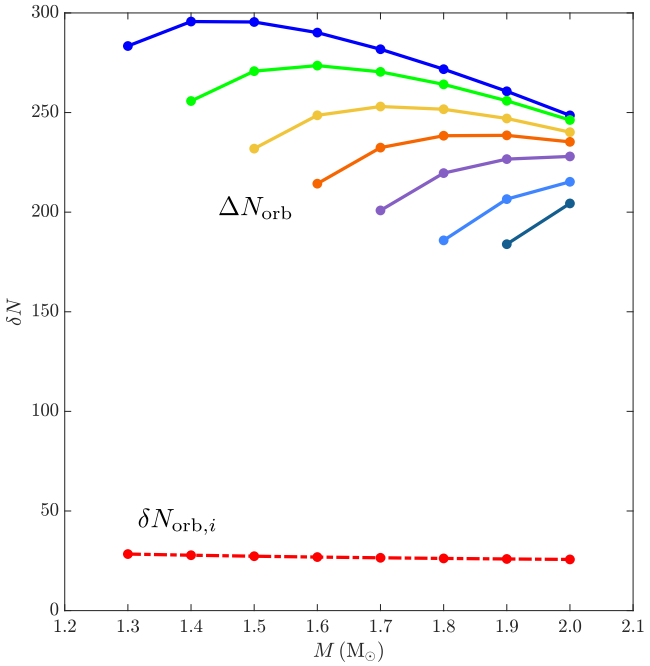

FIG. 15. Distinguishability of the NS and its HS counterpart at different masses. For illustrative purposes, the mass of the companion compact star is set to be fixed at $1.4M_\odot$. The red dashed line is the $\delta N_{\rm orb}$ of the i_μ-mode resonance of the NS. The solid lines are the differences in the orbital cycle between the NS-NS binary system and the NS-HS binary system's resonant orbital frequencies. Detailed analysis is in the main text.

$$\Delta N_{\rm orb} = \int_{t_1}^{t_2} \Omega(t) dt/2\pi, \tag{20}$$

where the $\Omega(t)$ can be solved from Eq. (9). The t_1 and t_2 are the moments when orbital frequencies take the value of f_1 and f_2, respectively. To distinguish NS/HS from the binary system, $f_{1/2}$ can take the value of half of the i_μ frequency for the NS/HS, that is, the orbital resonant frequency of the NS/HS, respectively. The NS/HS is distinguishable as long as the inequality $\Delta N_{\rm orb} > \delta N_{\rm orb}$ is satisfied.

In Fig. 15, we demonstrate the distinguishability of the HS solution compared with the NS solution based on NL3 EOS. Since there is no density discontinuity near the crust-core interface in the NL3 EOS, the corresponding frequency of the crust-core interfacial mode i_μ is around 30–40 Hz. Therefore, the orbital excitation of this i_μ-mode happens in a relatively early inspiral stage. Although the frequency differences between NSs and HSs are only about 7–10 Hz, the difference of the number of orbital cycles $\Delta N_{\rm orb}$ for the HS and NS is large enough compared with the $\delta N_{\rm orb}$, which indicates its possible detectability.

V. CONCLUSION AND OUTLOOK

In this work, we studied the possibility of using the crust-core interfacial mode of the neutron stars to probe the phase

transition in dense matter. Some phase transitions, in particular, those that can significantly change the mass-radius relation or the tidal deformability of the neutron stars, can be probed using electromagnetic observations or the adiabatic GW waveform. There could also exist phase transitions that have a minor effect on the M-R relation and the tidal deformability. For example, in the fluid core of a NS, first-order phase transitions with density discontinuity can happen near the crust-core interface, due to the possible emergence of the new baryon degrees of freedom. For these phase transitions, we explore the possibility of probing them using the crust-core interfacial mode, which can couple efficiently to the orbital motion of a binary neutron star system and leaves signatures in the gravitational wave radiations. In this work, we carefully analyzed the properties of the crust-core interfacial mode and found that they can be significantly modified by the existence of these first-order phase transitions. We also study the observability of this phase transition using Fisher analysis. Moreover, we also explore the effect of the hadron-quark phase transition on the interfacial mode and its possible observability in the gravitational wave signals, as complementary to the measurement of the M-R relation. Our results indicate that a ground-based gravitational wave detector has the potential to detect the signature of these phase transitions via the crust-core interfacial mode.

We want to comment that our results here may have the following inaccuracies. Firstly, our analysis was based on a Newtonian perturbation theory on a general relativistic background stellar structure under the Cowling approximation, where the perturbation of the gravitational field and its coupling to the perturbation of the fluid energy momentum were ignored for simplicity. The most accurate analysis should be based on a fully consistent general relativistic calculation. For neutron stars, applying Newtonian approximation usually contributes $\sim 10\%$ error on the value of the mode frequencies. This could be important because, as we have discussed before, a difference of a few Hz can correspond to many orbital cycles at low frequency. We leave the full relativistic perturbation calculation for a future work. Secondly, the detailed inelastic mechanical process of the neutron star crust under the excitation of the tidal interactions is not entirely clear [37,87] since it depends on the exotic matter phase in the extreme conditions in the neutron star. Therefore, the results concerning the inelastic effect of neutron star crust in this work should be valid as semiquantitative estimations. A more accurate understanding needs a more detailed study of the inelastic properties of the crust. Thirdly, our analysis is based on the binary system where the compact stars have no spin angular momentum, which, in principle, can affect the interfacial mode and the orbital motion. The spin affects the internal oscillation mode in a way similar to the Zeeman effect in atomic physics or the Sagnac effect in a laser gyroscope, and the orbital motion of the binary system can also be modulated due to the spin-orbital and spin-spin coupling. Besides, only near-circular binary orbit is considered, while, in principle, the interfacial mode can also be excited via an eccentric orbit. We leave the improvement of this work by dealing with these inaccuracies for future works.

ACKNOWLEDGMENTS

The authors devote many thanks to Professor Micaela Oertel, Dr. Helena Pais, and the "CompOSE" team for patient discussions and help in constructing a consistent neutron star EOS. Y. M. thanks Professor Huan Yang and Dr. Zhen Pan for the discussions on their work about the interfacial mode and for sharing their calculations for comparison. He also thanks Professor Shun Wang for his constant support. J. Z., C. W., and Y. M. thank Professor Yanbei Chen for the discussion and his encouragement in completing this work. We also thank Miss Zeying Xia for her administrative support. J. Z. is supported by China National Scholarship (undergraduates). E. Z. thanks Yong Gao for discussion on the g-mode. Y. M. is supported by the start-up funding provided by Huazhong University of Science and Technology. E. Z. is supported by National SKA Program of China No. 2020SKA0120300 and NSFC Grant No. 12203017. C. X. is supported by the National SKA Program of China (Grant No. 2020SKA0120300) and the National Natural Science Foundation of China (Grant No. 12275234).

APPENDIX A: SOME DETAILS ON SOLVING THE INTERFACIAL MODES

We follow the standard approach [69] to solve the eigenfrequencies of asteroseismology under the Cowling approximation, briefly summarized in this section. We also discuss some important numerical details.

In the solid crust, the movement of a mass element is governed by Newton's second law, mass continuity equation, and the Poisson equation for gravitational potential:

$$\frac{\partial \vec{v}}{\partial t} + (\vec{v}\cdot\nabla)\vec{v} = \frac{1}{\rho}\nabla\cdot\mathbb{S} - \nabla\Phi,$$
$$\frac{\partial \rho}{\partial t} + \nabla\cdot(\rho\vec{v}) = 0, \qquad \nabla^2\Phi = 4\pi G\rho, \tag{A1}$$

where $\mathbb{S}$ is the elastic stress tensor with component as

$$S_{ij} = \Gamma_1 P \mathrm{Tr}(\epsilon)\delta_{ij} + 2\mu\left[\epsilon_{ij} - \frac{1}{3}\mathrm{Tr}(\epsilon)\delta_{ij}\right], \tag{A2}$$

where $\epsilon_{ij} = (\xi_{i,j} + \xi_{j,i})/2$ is the strain tensor, μ is the shear modulus, and $\Gamma_1 = dlnP/dln\rho$ is the adiabatic index, which is a characterization of the matter hardness. In particular, we will see later that the eigenmode results are very sensitive to Γ, and we need to be careful in the

numerical treatment of Γ. For the fluid core, the equation is the same except the shear modulus μ is set to be zero.

Perturbations are applied to the above equations, with static zeroth order background quantities obtained using the Tolman-Oppenheimer-Volkoff equation. We do not list the cumbersome detailed form of the perturbation equations, which can be easily found in [34,35,37,69]; we only list the important junction conditions at different interfaces and other important details that need to be noticed.

1. Junction conditions

As mentioned in Sec. III, there are two different interfaces in the compact star: the shear-modulus discontinuity interface and the density discontinuity interface. When integrating across these interfaces, proper junction conditions must be applied to connect the perturbation variables at both sides of the interface.

The physical conditions, which must be satisfied at both interfaces, are the continuity of the radial displacement of the fluid elements and the radial stress. These two requirements are sufficient to construct the connection at the density discontinuity interface. At the shear-modulus interface, an additional condition acquiring zero shear stress means that an ideal fluid with $\mu = 0$ does not support shear stress.

The dimensionless perturbation variables of the solid crust that appear in the oscillation equations are

$$z_1 = \frac{U}{r}, \qquad z_2 = \frac{\lambda}{p}\left[\frac{1}{r^2}\frac{d}{dr}(r^2 U) - \frac{l(l+1)}{r}V\right] + 2\frac{\mu}{p}\frac{dU}{dr},$$
$$z_3 = \frac{V}{r}, \qquad z_4 = \frac{\mu}{p}\left(\frac{dV}{dr} - \frac{V}{r} + \frac{U}{r}\right), \tag{A3}$$

where $\lambda = \Gamma_1 p - 2/3\mu$ is the Lamé coefficient.

The dimensionless perturbation variables of the liquid core are

$$y_1 = \frac{U}{r}, \qquad y_2 = \frac{\delta p}{\rho g r}. \tag{A4}$$

Correspondingly, the junction conditions at the two interfaces are

$$[z_1]_{\text{solid}} = [y_1]_{\text{liquid}}$$
$$[z_2]_{\text{solid}} = [\tilde{V}(y_1 - y_2)]_{\text{liquid}}$$
$$[z_4]_{\text{solid}} = 0 \tag{A5}$$

and

$$y_{1l} = y_{1h},$$
$$\tilde{V}_l(y_{1l} - y_{2l}) = \tilde{V}_h(y_{1h} - y_{2h}). \tag{A6}$$

In the junction condition, there appears a quantity $\tilde{V} = -d\ln p/d\ln r = \rho g r/p$. Therefore, the density discontinuity will result in a discontinuity of $\tilde{V}$.

The brackets "[]" in the above formula with the subscripts "solid" and "liquid" indicate that the quantities should be evaluated at both solid and liquid sides, respectively. In (A6), the subscripts "l" and "h" indicate that the quantities should be evaluated at the lower mass density side and the higher mass density side, respectively, at the

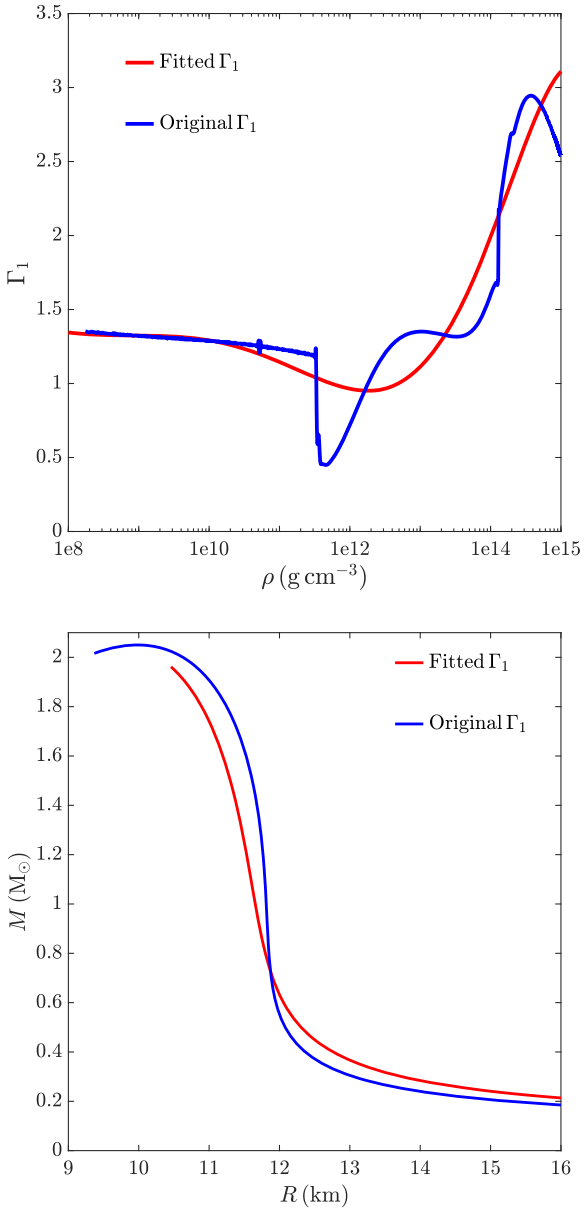

FIG. 16. The adiabatic index Γ_1 (upper panel) and the corresponding M-R relation (lower panel). The blue line is the Γ_1 of SLy4 EOS using a cubic spline interpolation algorithm [74], while the red line is the one using a polynomial interpolation algorithm. Although these two approaches fit quite well at the low density region, they are deviated from each other in the crust-core transition region. If the accuracy of the precision of the interpolation algorithm was not well controlled, then the resultant Γ_1 actually corresponds to a different EOS and hence a different TOV solution.

interface of the first-order phase transition in the liquid core, which is essential to the calculation of "free-slipping" effects.

2. Numerical details on the adiabatic index

The adiabatic index Γ_1 characterizes the stiffness of the EOS and reflects some physical effects like the softening of the EOS when the density is higher than the neutron drip density or the stiffening at the crust-core interface of SLy4 EOS. However, we need to be careful in choosing the algorithm when we obtain the adiabatic index. For example, using a 9-order polynomial interpolation to obtain the Γ_1, shown approximately in Fig. 16, will have some problems. First, this method may significantly alter the EOS stiffness behavior around the crust-core region, thereby removing some important physical facts that may affect the properties of the i-mode. Second, the altered Γ_1 essentially represents a new $P-\rho$ relation and thus a different EOS. It creates an artificial inconsistency with the original background static star solution computed by the original $P-\rho$ relation. Our test shows that this inconsistency will overestimate the i-mode frequency from 54 Hz to 170 Hz due to the increasing of Γ_1 at the crust-core region for the EOS SLy4 with $1.4M_\odot$.

APPENDIX B: CRUST MELTING

We follow the same approach as in [37] to compute the effect of crust melting to the binary neutron stars system, which is briefly summarized in this appendix section.

Once the tidal-induced shear strain exceeds the elastic limit $\epsilon_b \sim 0.1$, the plastic deformation of the crust will cause heat dissipation given by [88]

$$\dot{\epsilon}_{pl} = \frac{n_i Z^2 e^2 \omega_p}{a\mu \bar{N}\Gamma} e^{(-18.5\bar{\sigma}_b + \bar{\sigma}\bar{N})\Gamma}, \tag{B1}$$

where μ is the elastic shear modulus [89,90]:

$$\mu = \frac{0.1194}{1+0.595(173/\Gamma)^2}\frac{n_i(Ze)^2}{a}, \quad \text{with } n_i = \frac{N(1-X_n)}{A}. \tag{B2}$$

Here N is the baryon number density, X_n is the fraction of nucleons in the neutron gas [90], $a = (3/4\pi n_i)^{1/3}$ is the average ion spacing, $\omega_p = (4\pi Z^2 e^2 n_i/Am_b)^{1/2}$ is the ion plasma frequency, $\sigma = \mu\epsilon_{el}$ is the shear stress, $\bar{\sigma} = \sigma/(n_i Z^2 e^2/a)$, $\Gamma = (Ze)^2/ak_BT$ is the melting parameter, and for $\Gamma = \Gamma_m \approx 180$ the crust undergoes a fluid-solid transition. The melting temperature for the bottom of the crust is $T \sim 1$ MeV. Then the energy heating rate due to the plastic deformation is [87]

$$n_i \dot{e}_i = \sigma \dot{\epsilon}_{pl}(\sigma, T), \tag{B3}$$

where e_i is the thermal energy per ion. The energy dissipation rate has an exponential dependence on the elastic strain [see Eq. (B1)]. Therefore, we can expect that at some point during the evolution, the heating will become very fast.

For computing the heating effect $de_i = c_V dT$, we need the specific heat capacity per ion given as [91]

$$\frac{c_V}{k_B} = 8D_3(\alpha\eta) - 6\frac{\alpha\eta}{\alpha\eta - 1} + e^{\gamma_L}\eta\left(\frac{\gamma_L\eta}{e^{\gamma_L\eta}-1}\right)^2, \tag{B4}$$

where D_3 is the Debye integral, $\alpha = 0.4$, and $\eta = \hbar\omega_p/k_BT$ with ω_p the plasma frequency and T the temperature. The $\gamma_L = 0.899$ is the longitudinal correction factor of the acoustic mode in a Coulomb crystal defined in [92], which should be distinguished from the mode damping factor γ. We can get the time derivative of temperature: $\dot{T} = \mu\epsilon_{el}\dot{\epsilon}_{pl}/n_i c_V$. We mainly focus on the temperature evolution at the crust base for its dominant role in the crust heat capacity. The melting will affect the parameters of the interfacial mode, for example, the damping factor γ and the resonant frequency will depend on time, that is

$$\ddot{a}_m(t) + \gamma(t)\dot{a}_m(t) + \omega_m^2(t)a_m(t) = \frac{GM_* W_{2m} Q_{2m}}{D(t)^3} e^{-im\Phi(t)}. \tag{B5}$$

For example, the damping rate is

$$\gamma(t) \approx \left(2\int_{\text{crust}} d^3x n_i \dot{e}_i(t)\right) \Big/ \left(MR^2 \sum_m |\dot{a}_m(t)|^2 + \omega_m^2(t)|a_m(t)|^2\right), \tag{B6}$$

where the denominator represents the mode's total energy, and the numerator represents the total energy dissipation rate in the crust. The resonant frequency $\omega_\alpha(t)$ is assumed to be proportional to the square root of the shear modulus $\mu(t)$ in Eq. (B2), which also depends on the increasing temperature during the heating process. Combining the above equations, one can analyze how the melting process affects the coupling between the interfacial mode and the orbital motion, on which the lower panel of Fig. 14 is based.

[1] Paweł Danielewicz, Roy Lacey, and William G. Lynch, Determination of the equation of state of dense matter, Science **298**, 1592 (2002).

[2] V. Baran, M. Colonna, V. Greco, and M. Di Toro, Reaction dynamics with exotic nuclei, Phys. Rep. **410**, 335 (2005).

[3] W. G. Lynch, M. B. Tsang, Y. Zhang, P. Danielewicz, M. Famiano, Z. Li, and A. W. Steiner, Probing the symmetry energy with heavy ions, Prog. Part. Nucl. Phys. **62**, 427 (2009); Heavy-ion collisions from the Coulomb barrier to the quark-gluon plasma, *30th Course International Workshop on Nuclear Physics*.

[4] Bao-An Li, Lie-Wen Chen, and Che Ming Ko, Recent progress and new challenges in isospin physics with heavy-ion reactions, Phys. Rep. **464**, 113 (2008).

[5] Yingxun Zhang, Min Liu, Cheng-Jun Xia, Zhuxia Li, and S. K. Biswal, Constraints on the symmetry energy and its associated parameters from nuclei to neutron stars, Phys. Rev. C **101**, 034303 (2020).

[6] Agnieszka Sorensen *et al.*, Dense nuclear matter equation of state from heavy-ion collisions, arXiv:2301.13253v2.

[7] M. E. Caplan and C. J. Horowitz, Colloquium: Astromaterial science and nuclear pasta, Rev. Mod. Phys. **89**, 041002 (2017).

[8] D. G. Ravenhall, C. J. Pethick, and J. R. Wilson, Structure of Matter Below Nuclear Saturation Density, Phys. Rev. Lett. **50**, 2066 (1983).

[9] Masa-aki Hashimoto, Hironori Seki, and Masami Yamada, Shape of nuclei in the crust of neutron star, Prog. Theor. Phys. **71**, 320 (1984).

[10] Kazuhiro Oyamatsu, Masa-aki Hashimoto, and Masami Yamada, Further study of the nuclear shape in high-density matter, Prog. Theor. Phys. **72**, 373 (1984).

[11] R. D. Williams and S. E. Koonin, Sub-saturation phases of nuclear matter, Nucl. Phys. **A435**, 844 (1985).

[12] Andreas Bauswein, Niels-Uwe F. Bastian, David B. Blaschke, Katerina Chatziioannou, James A. Clark, Tobias Fischer, and Micaela Oertel, Identifying a First-Order Phase Transition in Neutron-Star Mergers through Gravitational Waves, Phys. Rev. Lett. **122**, 061102 (2019).

[13] Elias R. Most, L. Jens Papenfort, Veronica Dexheimer, Matthias Hanauske, Stefan Schramm, Horst Stöcker, and Luciano Rezzolla, Signatures of Quark-Hadron Phase Transitions in General-Relativistic Neutron-Star Mergers, Phys. Rev. Lett. **122**, 061101 (2019).

[14] Lukas R. Weih, Matthias Hanauske, and Luciano Rezzolla, Postmerger Gravitational-Wave Signatures of Phase Transitions in Binary Mergers, Phys. Rev. Lett. **124**, 171103 (2020).

[15] P. B. Demorest, T. Pennucci, S. M. Ransom, M. S. E. Roberts, and J. W. T. Hessels, A two-solar-mass neutron star measured using shapiro delay, Nature (London) **467**, 1081 (2010).

[16] John Antoniadis *et al.*, A massive pulsar in a compact relativistic binary, Science **340**, 1233232 (2013).

[17] Emmanuel Fonseca *et al.*, The nanograv nine-year data set: Mass and geometric measurements of binary millisecond pulsars, Astrophys. J. **832**, 167 (2016).

[18] H. Thankful Cromartie *et al.*, Relativistic shapiro delay measurements of an extremely massive millisecond pulsar, Nat. Astron. **4**, 72 (2020).

[19] E. Fonseca *et al.*, Refined mass and geometric measurements of the high-mass PSR j0740 + 6620. Astrophys. J. **915**, L12 (2021).

[20] LIGO Scientific and Virgo Collaborations, Gw170817: Measurements of Neutron Star Radii and Equation of State, Phys. Rev. Lett. **121**, 161101 (2018).

[21] T. E. Riley, A. L. Watts, S. Bogdanov, P. S. Ray, R. M. Ludlam, S. Guillot, Z. Arzoumanian, C. L. Baker, A. V. Bilous, D. Chakrabarty, K. C. Gendreau, A. K. Harding, W. C. G. Ho, J. M. Lattimer, S. M. Morsink, and T. E. Strohmayer, A nicer view of psr j0030 + 0451: Millisecond pulsar parameter estimation, Astrophys. J. **887**, L21 (2019).

[22] Thomas E. Riley *et al.*, A NICER view of the massive pulsar PSR j0740 + 6620 informed by radio timing and XMM-newton spectroscopy, Astrophys. J. **918**, L27 (2021).

[23] M. C. Miller *et al.*, Psr j0030 + 0451 mass and radius from nicer data and implications for the properties of neutron star matter, Astrophys. J. **887**, L24 (2019).

[24] M. C. Miller *et al.*, The radius of PSR j0740 + 6620 from NICER and XMM-newton data, Astrophys. J. **918**, L28 (2021).

[25] B. P. Abbott, R. Abbott, T. D. Abbott, F. Acernese, K. Ackley, C. Adams, T. Adams, P. Addesso, R. X. Adhikari, V. B. Adya *et al.*, GW170817: Measurements of Neutron Star Radii and Equation of State, Phys. Rev. Lett. **121**, 161101 (2018).

[26] B. P. Abbott, R. Abbott, T. D. Abbott, F. Acernese, K. Ackley, C. Adams, T. Adams, P. Addesso, R. X. Adhikari, V. B. Adya *et al.*, Properties of the Binary Neutron Star Merger GW170817, Phys. Rev. X **9**, 011001 (2019).

[27] E. Annala, T. Gorda, A. Kurkela, and A. Vuorinen, Gravitational-Wave Constraints on the Neutron-Star-Matter Equation of State, Phys. Rev. Lett. **120**, 172703 (2018).

[28] Soumi De, Daniel Finstad, James M. Lattimer, Duncan A. Brown, Edo Berger, and Christopher M. Biwer, Tidal Deformabilities and Radii of Neutron Stars from the Observation of GW170817, Phys. Rev. Lett. **121**, 091102 (2018).

[29] M. Ruiz, S. L. Shapiro, and A. Tsokaros, GW170817, general relativistic magnetohydrodynamic simulations, and the neutron star maximum mass, Phys. Rev. D **97**, 021501 (2018).

[30] L. Rezzolla, E. R. Most, and L. R. Weih, Using gravitational-wave observations and quasi-universal relations to constrain the maximum mass of neutron stars, Astrophys. J. Lett. **852**, L25 (2018).

[31] Masaru Shibata, Enping Zhou, Kenta Kiuchi, and Sho Fujibayashi, Constraint on the maximum mass of neutron stars using GW170817 event, Phys. Rev. D **100**, 023015 (2019).

[32] B. Margalit and B. D. Metzger, Constraining the maximum mass of neutron stars from multi-messenger observations of GW170817, Astrophys. J. Lett. **850**, L19 (2017).

[33] A. Bauswein, O. Just, H.-T. Janka, and N. Stergioulas, Neutron-star radius constraints from GW170817 and future detections, Astrophys. J. Lett. **850**, L34 (2017).

[34] Shu Yan Lau and Kent Yagi, Probing hybrid stars with gravitational waves via interfacial modes, Phys. Rev. D **103**, 063015 (2021).

[35] P. N. McDermott, H. M. van Horn, and C. J. Hansen, Nonradial oscillations of neutron stars, Astrophys. J. **325**, 725 (1988).
[36] David Tsang, Jocelyn S. Read, Tanja Hinderer, Anthony L. Piro, and Ruxandra Bondarescu, Resonant Shattering of Neutron Star Crusts, Phys. Rev. Lett. **108**, 011102 (2012).
[37] Zhen Pan, Zhenwei Lyu, Béatrice Bonga, Néstor Ortiz, and Huan Yang, Probing Crust Meltdown in Inspiraling Binary Neutron Stars, Phys. Rev. Lett. **125**, 201102 (2020).
[38] Mark G. Alford, Sophia Han, and Madappa Prakash, Generic conditions for stable hybrid stars, Phys. Rev. D **88**, 083013 (2013).
[39] C. J. Krüger, W. C. G. Ho, and N. Andersson, Seismology of adolescent neutron stars: Accounting for thermal effects and crust elasticity, Phys. Rev. D **92**, 063009 (2015).
[40] Zhiqiang Miao, Ang Li, Zhenyu Zhu, and Sophia Han, Constraining hadron-quark phase transition parameters within the quark-mean-field model using multimessenger observations of neutron stars, Astrophys. J. **904**, 103 (2020).
[41] Aleksi Kurkela, Paul Romatschke, Aleksi Vuorinen, and Bin Wu, Looking inside neutron stars: Microscopic calculations confront observations, arXiv:1006.4062.
[42] Mark G. Alford, G. F. Burgio, S. Han, G. Taranto, and D. Zappalà, Constraining and applying a generic high-density equation of state, Phys. Rev. D **92**, 083002 (2015).
[43] Gordon Baym, Tetsuo Hatsuda, Toru Kojo, Philip D. Powell, Yifan Song, and Tatsuyuki Takatsuka, From hadrons to quarks in neutron stars: A review, Rep. Prog. Phys. **81**, 056902 (2018).
[44] G. Baym and S. A. Chin, Can a neutron star be a giant mit bag?, Phys. Lett. **62B**, 241 (1976).
[45] M. Fortin, C. Providência, Ad. R. Raduta, F. Gulminelli, J. L. Zdunik, P. Haensel, and M. Bejger, Neutron star radii and crusts: Uncertainties and unified equations of state, Phys. Rev. C **94**, 035804 (2016).
[46] G. A. Lalazissis, J. König, and P. Ring, New parametrization for the lagrangian density of relativistic mean field theory, Phys. Rev. C **55**, 540 (1997).
[47] P.-G. Reinhard and H. Flocar, Nuclear effective forces and isotope shifts, Nucl. Phys. **A584**, 467 (1995).
[48] J. Friedrich and P.-G. Reinhard, Skyrme-force parametrization: Least-squares fit to nuclear ground-state properties, Phys. Rev. C **33**, 335 (1986).
[49] E. Chabanat, P. Bonche, P. Haensel, J. Meyer, and R. Schaeffer, A skyrme parametrization from subnuclear to neutron star densities part ii. nuclei far from stabilities, Nucl. Phys. **A635**, 231 (1998).
[50] A. Akmal, V. R. Pandharipande, and D. G. Ravenhall, Equation of state of nucleon matter and neutron star structure, Phys. Rev. C **58**, 1804 (1998).
[51] S. Typel, G. Röpke, T. Klähn, D. Blaschke, and H. H. Wolter, Composition and thermodynamics of nuclear matter with light clusters, Phys. Rev. C **81**, 015803 (2010).
[52] Fabrizio Grill, Helena Pais, Constan ça Providência, Isaac Vidaña, and Sidney S. Avancini, Equation of state and thickness of the inner crust of neutron stars, Phys. Rev. C **90**, 045803 (2014).
[53] G. A. Lalazissis, T. Nikšić, D. Vretenar, and P. Ring, New relativistic mean-field interaction with density-dependent meson-nucleon couplings, Phys. Rev. C **71**, 024312 (2005).
[54] Cheng-Jun Xia, Toshiki Maruyama, Ang Li, Bao Yuan Sun, Wen-Hui Long, and Ying-Xun Zhang, Unified neutron star eoss and neutron star structures in rmf models, Commun. Theor. Phys. **74**, 095303 (2022).
[55] Cheng-Jun Xia, Bao Yuan Sun, Toshiki Maruyama, Wen-Hui Long, and Ang Li, Unified nuclear matter equations of state constrained by the in-medium balance in density-dependent covariant density functionals, Phys. Rev. C **105**, 045803 (2022).
[56] S. Typel and H. H. Wolter, Relativistic mean field calculations with density-dependent meson-nucleon coupling, Nucl. Phys. **A656**, 331 (1999).
[57] Bin Wei, Qiang Zhao, Zhi-Heng Wang, Jing Geng, Bao-Yuan Sun, Yi-Fei Niu, and Wen-Hui Long, Novel relativistic mean field lagrangian guided by pseudo-spin symmetry restoration *, Chin. Phys. C **44**, 074107 (2020).
[58] N. Chamel, Analytical determination of the structure of the outer crust of a cold nonaccreted neutron star, Phys. Rev. C **101**, 032801 (2020).
[59] S. Antić, J. R. Stone, J. C. Miller, K. L. Martinez, P. A. M. Guichon, and A. W. Thomas, Outer crust of a cold, non-accreting neutron star within the quark-meson-coupling model, Phys. Rev. C **102**, 065801 (2020).
[60] A. Pastore, D. Neill, H. Powell, K. Medler, and C. Barton, Impact of statistical uncertainties on the composition of the outer crust of a neutron star, Phys. Rev. C **101**, 035804 (2020).
[61] M. E. Caplan, Andrew Cumming, D. K. Berry, C. J. Horowitz, and R. Mckinven, Polycrystalline crusts in accreting neutron stars, Astrophys. J. **860**, 148 (2018).
[62] Gordon Baym, Tetsuo Hatsuda, Toru Kojo, Philip D. Powell, Yifan Song, and Tatsuyuki Takatsuka, From hadrons to quarks in neutron stars: A review, Rep. Prog. Phys. **81**, 056902 (2018).
[63] Ting-Ting Sun, Shi-Sheng Zhang, Qiu-Lan Zhang, and Cheng-Jun Xia, Strangeness and Δ resonance in compact stars with relativistic-mean-field models, Phys. Rev. D **99**, 023004 (2019).
[64] Eemeli Annala, Tyler Gorda, Aleksi Kurkela, Joonas Nättilä, and Aleksi Vuorinen, Evidence for quark-matter cores in massive neutron stars, Nat. Phys. **16**, 907 (2020).
[65] V. Dexheimer, R. O. Gomes, T. Klähn, S. Han, and M. Salinas, GW190814 as a massive rapidly rotating neutron star with exotic degrees of freedom, Phys. Rev. C **103**, 025808 (2021).
[66] Hung Tan, Travis Dore, Veronica Dexheimer, Jacquelyn Noronha-Hostler, and Nicolás Yunes, Extreme matter meets extreme gravity: Ultraheavy neutron stars with phase transitions, Phys. Rev. D **105**, 023018 (2022).
[67] A. Akmal, V. R. Pandharipande, and D. G. Ravenhall, Equation of state of nucleon matter and neutron star structure, Phys. Rev. C **58**, 1804 (1998).
[68] Wen-Jie Xie and Bao-An Li, Bayesian inference of the dense-matter equation of state encapsulating a first-order hadron-quark phase transition from observables of canonical neutron stars, Phys. Rev. C **103**, 035802 (2021).
[69] P. N. McDermott, H. M. van Horn, and C. J. Hansen, Nonradial oscillations of neutron stars, Astrophys. J. **325**, 725 (1988).

[70] Bonny L. Schumaker and Kip S. Thorne, Torsional oscillations of neutron stars, Mon. Not. R. Astron. Soc. **203**, 457 (1983).
[71] C. J. Hansen and D. F. Cioffi, Torsional oscillations in neutron star crusts, Astrophys. J. **238**, 740 (1980).
[72] A. Passamonti and N. Andersson, Towards real neutron star seismology: Accounting for elasticity and superfluidity, Mon. Not. R. Astron. Soc. **419**, 638 (2012).
[73] A. Passamonti, N. Andersson, and P. Pnigouras, Dynamical tides in neutron stars: The impact of the crust, Mon. Not. R. Astron. Soc. **504**, 1273 (2021).
[74] William H. Press, Saul A. Teukolsky, William T. Vetterling, and Brian P. Flannery, *Numerical Recipes in C*, 2nd ed. (Cambridge University Press, Cambridge, USA, 1992).
[75] Kip S. Thorne and Roger D. Blandford, *Modern Classical Physics Optics, Fluids, Plasmas, Elasticity, Relativity, and Statistical Physics* (Princeton University Press, 2018), p. 782.
[76] S. Typel, M. Oertel, and T. Klähn, CompOSE CompStar online supernova equations of state harmonising the concert of nuclear physics and astrophysics compose.obspm.fr, Phys. Part. Nucl. **46**, 633 (2015).
[77] M. Oertel, M. Hempel, T. Klähn, and S. Typel, Equations of state for supernovae and compact stars, Rev. Mod. Phys. **89**, 015007 (2017).
[78] S. Typel, M. Oertel, T. Klähn, D. Chatterjee, V. Dexheimer, C. Ishizuka, M. Mancini, J. Novak, H. Pais, C. Providencia, A. Raduta, M. Servillat, and L. Tolos, Compose reference manual, Eur. Phys. J. **58**, 221 (2022).
[79] Tuhin Malik and Helena Pais, Inner crust equations of state for CompOSE, Eur. Phys. J. A **58**, 8 (2022).
[80] Éanna É. Flanagan and Étienne Racine, Gravitomagnetic resonant excitation of rossby modes in coalescing neutron star binaries, Phys. Rev. D **75**, 044001 (2007).
[81] Sizheng Ma, Hang Yu, and Yanbei Chen, Detecting resonant tidal excitations of rossby modes in coalescing neutron-star binaries with third-generation gravitational-wave detectors, Phys. Rev. D **103**, 063020 (2021).
[82] Dong Lai, Resonant oscillationsand tidal heating in coalescing binary neutron stars, Mon. Not. R. Astron. Soc. **270**, 611 (1994).
[83] Curt Cutler and Éanna E. Flanagan, Gravitational waves from merging compact binaries: How accurately can one extract the binary's parameters from the inspiral waveform?, Phys. Rev. D **49**, 2658 (1994).
[84] Hang Yu and Nevin N. Weinberg, Resonant tidal excitation of superfluid neutron stars in coalescing binaries, Mon. Not. R. Astron. Soc. **464**, 2622 (2017).
[85] The LIGO Scientific Collaboration, Advanced LIGO, Classical Quantum Gravity **32**, 074001 (2015).
[86] Sheila Dwyer, Daniel Sigg, Stefan W. Ballmer, Lisa Barsotti, Nergis Mavalvala, and Matthew Evans, Gravitational wave detector with cosmological reach, Phys. Rev. D **91**, 082001 (2015).
[87] Christopher Thompson, Huan Yang, and Néstor Ortiz, Global crustal dynamics of magnetars in relation to their bright x-ray outbursts, Astrophys. J. **841**, 54 (2017).
[88] A. I. Chugunov and C. J. Horowitz, Breaking stress of neutron star crust, Mon. Not. R. Astron. Soc. **407**, L54 (2010).
[89] David Tsang, Jocelyn S. Read, Tanja Hinderer, Anthony L. Piro, and Ruxandra Bondarescu, Resonant Shattering of Neutron Star Crusts, Phys. Rev. Lett. **108**, 011102 (2012).
[90] Duncan Neill, William G. Newton, and David Tsang, Resonant shattering flares as multimessenger probes of the nuclear symmetry energy, Mon. Not. R. Astron. Soc. **504**, 1129 (2021).
[91] Gilles Chabrier, Quantum effects in dense coulombic matter: Application to the cooling of white dwarfs, Astrophys. J. **414**, 695 (1993).
[92] Duncan Neill, William G. Newton, and David Tsang, Resonant shattering flares as multimessenger probes of the nuclear symmetry energy, Mon. Not. R. Astron. Soc. **504**, 1129 (2021).